A&A 646, A21 (2021)
https://doi.org/10.1051/0004-6361/202038350

Astronomy & Astrophysics

The ExoMolOP database: Cross sections and *k*-tables for molecules of interest in high-temperature exoplanet atmospheres⋆

Katy L. Chubb[1,2], Marco Rocchetto[2], Sergei N. Yurchenko[2], Michiel Min[1], Ingo Waldmann[2], Joanna K. Barstow[2], Paul Mollière[3], Ahmed F. Al-Refaie[2], Mark W. Phillips[4], and Jonathan Tennyson[2]

[1] SRON Netherlands Institute for Space Research, Sorbonnelaan 2, 3584, CA, Utrecht, The Netherlands
e-mail: k.l.chubb@sron.nl
[2] Department of Physics and Astronomy, University College London, London WC1E 6BT, UK
e-mail: katy.chubb.14@ucl.ac.uk
[3] Max-Planck-Institut für Astronomie, Königstuhl 17, 69117 Heidelberg, Germany
[4] Astrophysics Group, School of Physics, University of Exeter, Stocker Road, Exeter EX4 4QL, UK

Received 5 May 2020 / Accepted 28 August 2020

ABSTRACT

Here we present a publicly available database of opacities for molecules of astrophysical interest named ExoMolOP that has been compiled for over 80 species, and is based on the latest line list data from the ExoMol, HITEMP, and MoLLIST databases. These data are generally suitable for characterising high-temperature exoplanet or cool stellar and substellar atmospheres, and have been computed at a variety of pressures and temperatures, with a few molecules included at room temperature only from the HITRAN database. The data are formatted in different ways for four different exoplanet atmosphere retrieval codes; ARCiS, TauREx, NEMESIS, and petitRADTRANS, and include both cross sections (at $R = \frac{\lambda}{\Delta\lambda} = 15\,000$) and *k*-tables (at $R = \frac{\lambda}{\Delta\lambda} = 1000$) for the 0.3–50 μm wavelength region. Opacity files can be downloaded and used directly for these codes. Atomic data for alkali metals Na and K are also included, using data from the NIST database and the latest line shapes for the resonance lines. Broadening parameters have been taken from the literature where available, or have been estimated from the parameters of a known molecule with similar molecular properties where no broadening data are available.

Key words. molecular data – opacity – radiative transfer – planets and satellites: atmospheres – planets and satellites: gaseous planets – infrared: planetary systems

1. Introduction

There is now a large amount of molecular line list data available for characterising hot exoplanet or cool stellar/substellar atmospheres, largely due to databases such as ExoMol (Tennyson & Yurchenko 2012; Tennyson et al. 2016), HITEMP (Rothman et al. 2010; Hargreaves et al. 2019), MoLLIST (Bernath 2020), and TheoReTs (Rey et al. 2016). Line lists are independent of temperature and pressure, and so provide the most efficient way of storing the information required for characterising high-temperature astrophysical atmospheres. In order to convert this line list data into opacities (cross sections or *k*-tables), software such as ExoCross (Yurchenko et al. 2018a) is required to convert a pressure and temperature independent line list to cross-section data at a particular pressure and temperature. If a large number of pressures and temperatures are required for a large number of molecules, this can be a computationally demanding task. The present opacity database was formed in order to help reduce the computational effort of the community and to allow quick download and use of the data for many molecules designed specifically for use in atmospheric retrieval codes. The data are stored in formats which are exactly compatible for use with four different retrieval codes; ARCiS (Min et al. 2020), TauREx (Waldmann et al. 2015a,b; Al-Refaie et al. 2019), NEMESIS (Irwin et al. 2008), and petitRADTRANS (Mollière et al. 2019). Retrieval codes such as these have their own processes for the computation of opacities, but have previously been limited to a subsection of the molecules for which data are available. The data format required to input the opacities into each retrieval code is detailed in Sect. 4, with the intention that the data files are sufficiently easy to manipulate and reformat for use in any general retrieval code. There are tools available online, such as the exo-k library[1] (Leconte et al., in prep.), which enable conversion between different formats, some of which are those used in this work. Many other works have computed opacities for use in radiative-transfer retrieval and atmospheric modelling codes; see, for example, Showman et al. (2009), Freedman et al. (2008, 2014), Lee et al. (2019), Amundsen et al. (2014), Kempton et al. (2017), Grimm & Heng (2015), Malik et al. (2019), Kitzmann et al. (2020), Allard et al. (2012), Sharp & Burrows (2007), Line et al. (2013), Gandhi & Madhusudhan (2017), Phillips et al. (2020), Jørgensen (1998), Kurucz & Bell (1995).

The database of cross sections and *k*-tables presented in this work were used in a recent study by Chubb et al. (2020a), who re-examined the transmission spectra of "Hot Jupiter" exoplanet WASP-43b. These authors found that AlO, which had not previously been considered in similar analyses of the transmission spectra (Kreidberg et al. 2014; Stevenson et al. 2017; Fisher & Heng 2018; Tsiaras et al. 2018; Weaver et al. 2019; Irwin et al. 2020), was the molecule that fitted the data to the highest level of confidence out of all molecules for which high-temperature opacity data currently exist in the infra-red region covered by the HST WFC3 instrument

⋆ The data are available from www.exomol.com.

[1] http://perso.astrophy.u-bordeaux.fr/~jleconte/exo_k-doc/index.html

(Bean 2013). Other molecules with absorption features in this 1.1–1.7 μm region include C_2H_2, HCN, FeH, NH_3, ScH, VO, and TiH (Tennyson & Yurchenko 2018). Opacities from this database have also been used in works related to the investigation of ions in the thermospheres of planets (Bourgalais et al. 2020), the modelling of brown dwarf atmospheres (Lee et al. 2020), and other works related to exoplanet atmospheres (Taylor et al., in prep.; Min et al. 2020).

This paper is structured as follows. Section 2 gives an introduction to the line lists used in the present database and their data format. Section 3 discusses the computation of cross sections and k-tables from these line lists, including details of line broadening parameters used for each species in Sect. 3.2. Section 4 gives an overview of the four retrieval codes for which these opacities are formatted, and the data format specifications of each opacity file. The line list sources used for each species and their properties are detailed in Sect. 5, with comments in Sect. 5.1, and isotopologues in Sect. 5.2. The wavelength coverage of the database is briefly discussed in Sect. 6. Section 7 summarises the ExoMolOP database, including access and upkeep. The opacity requirements for high-resolution studies are discussed in Sect. 8. We give our conclusions in Sect. 9.

2. Line lists

2.1. Sources

HITRAN (Gordon et al. 2017) is a database of largely experimental data taken at room temperature. For this reason, although it is often very accurate – more accurate than theoretically calculated data – it is not considered complete (many of the weaker lines in particular are missing); it is only designed for temperatures in the region of 296 K although in practice HITRAN should work satisfactorily for temperatures below this. The GEISA database (Jacquinet-Husson et al. 2016) has similar properties to HITRAN. In order to characterise high-temperature atmospheres, such as those of exoplanets and stars, theoretical calculations need to be used in order to compute energy levels up to high energies, along with the Einstein-A coefficients between them (giving the probability of a transition between two states). Large projects and associated databases which contain line list data appropriate up to much higher temperatures (at least 1000 K) have therefore been set up to this effect. These include ExoMol (Tennyson & Yurchenko 2012; Tennyson et al. 2016), HITEMP (Rothman et al. 2010; Hargreaves et al. 2019), MoLLIST (Bernath 2020), along with TheoReTS (Rey et al. 2016), SPECTRA (Mikhailenko & Babikov 2005), MeCaSDA, and ECaSDa (Ba et al. 2013). It should be noted that a small number of molecules in the HITRAN database (HF, HCl, HBr, HI, H_2) are considered applicable up to high temperatures of around 4000–5000 K (Li et al. 2013). The data for this work were sourced mainly though the ExoMol database, with additions from HITEMP and MoLLIST (and HITRAN for the above-mentioned molecules for which data are appropriate up to 5000 K) where data are not currently available from ExoMol, or where they are more complete and therefore recommended for use from a different source. Atomic data are taken from the NIST database (Kramida et al. 2013), with original doublet data measured by Juncar et al. (1981) and Falke et al. (2006).

2.2. Data format

As stated above, the main data sources for this work are ExoMol, HITEMP/HITRAN, and MoLLIST. The data format of ExoMol line lists is explained in detail by Tennyson et al. (2013, 2016), with a 2020 update in Tennyson et al. (2020). A summary of the format is given below:

- A ".states" file, giving a unique set of energy levels for each molecule, along with a full set of quantum numbers;
- a ".trans" file, giving the transition probabilities between allowed energy states, in the form of Einstein-A coefficients;
- (for some molecules) a ".broad" file, describing the broadening parameters (typically for self, air, H_2 , or He broadening) for the transitions, as a function of rotational quantum number J;
- a ".pf" file, giving the temperature-dependent partition function.

The HITRAN and HITEMP data format, on the other hand, consists of one transition file per molecule with each line in the file representing one transition (i.e. one line of the spectra). All the quantum numbers for the upper- and lower-energy states are contained on this same line, along with any broadening parameters. This format works for HITRAN and HITEMP databases due to their much smaller size in comparison to ExoMol line lists. The number of lines in an ExoMol line list is typically many billion for larger polyatomic molecules, and therefore it not feasible to store such a large amount of data in HITRAN/HITEMP format.

3. Computing opacities

3.1. Cross sections

In order to compute cross sections from these line lists, we made use of ExoCross (Yurchenko et al. 2018a), which is a Fortran code for generating spectra (absorption and emission) and thermodynamic properties from molecular line lists, and accepts several formats including those of ExoMol and HITRAN/HITEMP. It produces cross sections at a specified resolution (or number of points), and broadening parameters can be included, with a variety of line broadening schemes available (see Sect. 3.2). The MoLLIST data used in this work were converted to ExoMol format by Wang et al. (2020). ExoCross is also capable of working with the super-lines method of Rey et al. (2016); see Sect. 3.2.4.

The partition functions for those species with data from HITRAN or HITEMP were mainly computed using TIPS (Total Internal Partition Sums) from Gamache et al. (2017), while for data which taken from the online ExoMol portal[2], the partition function provided there was used.

Rocchetto (2017) found that while a sampling resolving power of $R = \frac{\lambda}{\Delta\lambda} = 10\,000$ was sufficient to retrieve WFC3/HST spectra, a resolving power of at least 15 000 is needed to model JWST spectra. We therefore used $R = 15\,000$ for the cross-section data presented in this work. This resolution is still insufficient for high- resolution Doppler shift studies; for this see the recent work by Gandhi et al. (2020).

The cross sections for each species are computed at the grid of 27 temperature and 22 pressures as given by Table 1, giving a total of 594 temperature–pressure combinations for each molecule. The minimum and maximum wavelength values at which cross sections are computed is between 0.3 and 50 μm (200 - 33333 cm^{-1}), although not all molecules have this wide coverage (see Tables 7–14 in Sect. 5). Figures 1 and 2 provide an illustration of H_2O cross sections using the POKAZATEL line list (Polyansky et al. 2018) computed at a variety of pressures for $T = 1000$ K and a variety of temperatures for $P = 0.1$ bar,

[2] www.exomol.com

Table 1. Temperatures and pressures at which the cross sections and *k*-tables presented in this work are calculated.

Temperatures (K)	100	200	300	400	500	600
	700	800	900	1000	1100	1200
	1300	1400	1500	1600	1700	1800
	1900	2000	2200	2400	2600	2800
	3000	3200	3400			
Pressures (bar)	1×10^{-5}	2.1544×10^{-5}		4.6416×10^{-5}		
	1×10^{-4}	2.1544×10^{-4}		4.6416×10^{-4}		
	1×10^{-3}	2.1544×10^{-3}		4.6416×10^{-3}		
	1×10^{-2}	2.1544×10^{-2}		4.6416×10^{-2}		
	1×10^{-1}	2.1544×10^{-1}		4.6416×10^{-1}		
	1	2.1544		4.6416		
	10	21.544		46.416		
	100					

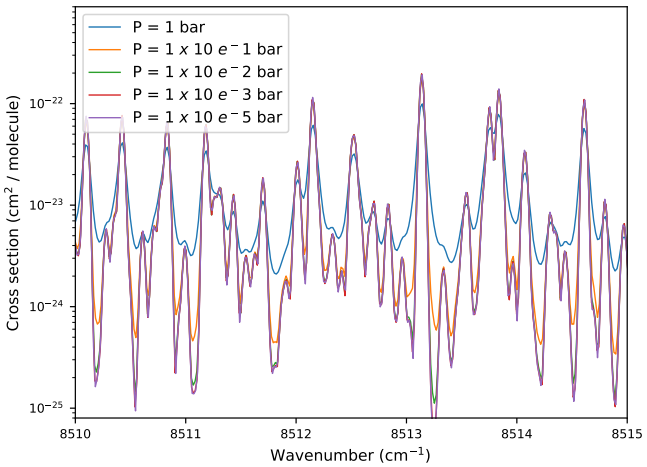

Fig. 1. H_2O broadened by H_2 and He (using the parameters of Table 2) at a variety of pressures for $T = 1000$ K.

respectively. The broadening parameters of Table 2 are used, assuming a solar H_2:He ratio (see Sect. 3.2).

Different errors resulting from various aspects of computed cross sections have been explored by Hedges & Madhusudhan (2016), Rocchetto (2017), Gharib-Nezhad & Line (2019) and Barstow et al. (2020). Differences largely arise from either the choice of line list for a particular species, or from the different treatments of the broadening of the lines, including line-wing cut-offs. The differences resulting from broadening type (i.e. self- compared to H_2 / He broadening) are thought to be significant for some species, such as H_2O, but not so much for others like CH_4, CO_2, or CO (Gharib-Nezhad & Line 2019).

It is well-known that a higher sampling of spectral lines leads to improvements in the accuracy of the opacity. Every line being very well sampled is equivalent to *line-by-line* integration. However, sampling cross sections at a lower resolution is far more computationally feasible for atmospheric retrievals. Retrieval results using cross sections have been found to be generally good when the sampling resolution is around two orders of magnitude higher than the resolution of the observed spectrum (Rocchetto 2017). For this work, high-resolution cross sections were first computed for each pressure–temperature grid point (as determined by Table 1) and then sampled to a lower resolution

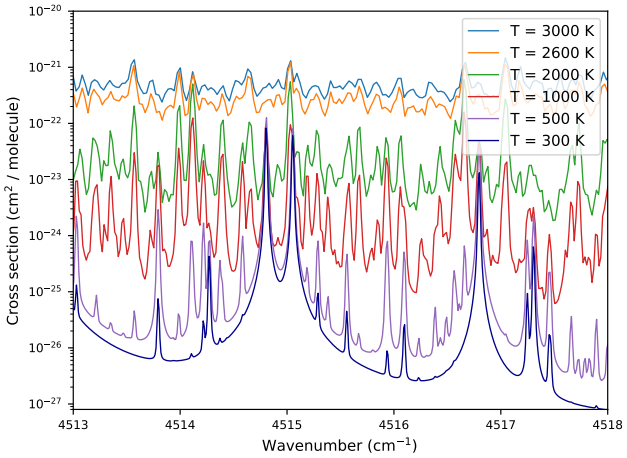

Fig. 2. H_2O broadened by H_2 and He (using the parameters of Table 2) at a variety of temperatures for $P = 0.1$ bar.

cross section or *k*-tables (see Sect. 3.3). The line broadening parameters used for these high-resolution cross sections are discussed in Sect. 3.2. For some molecules, such as those with many millions or billions of lines, the super-lines method was used (see Sect. 3.2.4), which has been found to vastly improve efficiency of calculations, and yields a very small error transmission provided a sufficiently fine grid is used (Yurchenko et al. 2017a).

See Sect. 3.2 for a summary of the method used to try and ensure an adequate number of sampling points for the Voigt-broadened high-resolution cross sections, depending on wavelength region, pressure, and temperature.

3.2. Line broadening

A line list can be used to compute a simple stick spectra; a temperature-dependent list of line positions and line intensities. However, a real spectrum will always have some broadening of these spectral lines due to various processes. The dominant type of line broadening in an exoplanet or stellar atmosphere are Doppler (thermal) and pressure broadening. Doppler broadening, which is temperature-dependent, arises because of the thermal velocities of individual molecules, and is represented by a Gaussian line profile (see, e.g. Yurchenko et al. 2018a):

$$f^D_{\tilde{\nu}_{fi},\alpha_D}(\tilde{\nu}) = \sqrt{\frac{\ln 2}{\pi}} \frac{1}{\alpha_D} \exp\left(-\frac{(\tilde{\nu} - \tilde{\nu}_{fi})^2 \ln 2}{\alpha_D^2}\right), \quad (1)$$

where $\tilde{\nu}_{fi}$ is the position of the line centre and α_D is the Doppler half-width at half-maximum (HWHM), as given by:

$$\alpha_D = \sqrt{\frac{2k_B T \ln 2}{m}} \frac{\tilde{\nu}_{fi}}{c} \quad (2)$$

for a molecule of mass m, at temperature T, and with k_B and c representing the Boltzmann constant and speed of light, respectively.

Pressure broadening, which is dependent on the perturbing species (commonly H, He, air or self) as well as the pressure, leads to a Lorentzian profile, as given by:

$$f^L_{\tilde{\nu}_{fi},\gamma_L}(\tilde{\nu}) = \frac{1}{\pi} \frac{\gamma_L}{(\tilde{\nu} - \tilde{\nu}_{fi})^2 + \gamma_L^2}, \quad (3)$$

where the Lorentzian line width (HWHM) is given by:

$$\gamma_L = \gamma_L^0 \left(\frac{T_0}{T}\right)^{n_L} \frac{P}{P_0}. \quad (4)$$

Table 2. Molecular properties for the species with computed opacities presented in this work for which H_2 and He broadening parameters are available in the literature, the majority of which were collated by Barton et al. (2017a).

Species	γ_{H_2}	n_{H_2}	γ_{He}	n_{He}	DM (d)	MM (g mol^{-1})	AN	Structure	Dipole Ref
H_2	0.01	0.13	0.01	0.13	0	2.0	2	Nonpolar	Johnson-III (2019)
CH_4	0.06	0.60	0.03	0.30	0	16.0	10	Nonpolar	
C_2H_2	0.09	0.59	0.04	0.44	0	26.0	14	Linear	
CO	0.07	0.65	0.05	0.60	0.1	28.0	14	Diatomic	Johnson-III (2019)
PH_3	0.10	0.75	0.05	0.30	0.6	34.0	18	Non-linear	
OCS	0.05	0.75	0.04	0.75	0.7	60.1	30	Linear	Dijkerman & Ruitenberg (1969)
HCl	0.03	0.75	0.01	0.75	1.1	36.5	18	Diatomic	Johnson-III (2019)
NH_3	0.08	0.50	0.03	0.50	1.5	17.0	10	Non-linear	
SO_2	0.14	0.75	0.07	0.64	1.6	64.1	32	Non-linear	
H_2O	0.06	0.20	0.01	0.13	1.9	18.0	10	Non-linear	
HF	0.04	0.75	0.01	0.50	1.9	20.0	10	Diatomic	Johnson-III (2019)
H_2CO	0.14	0.50	0.06	0.50	2.3	30.0	16	Non-linear	
HCN	0.12	0.50	0.05	0.50	3.0	27.0	14	Linear	Tomasevich (1970)

Notes. γ_x and n_x (where x = H or He) are the broadening parameters for hydrogen and helium (γ_0 and n_L in Eq. (4)). DM is the dipole moment, MM is the molar mass, and AN is the atomic number. The citations for the H_2/He broadening parameters are given below the table for each molecule. An average value for all values of J is taken for each set of broadening parameters. The reference temperature of T_0 = 296 K is used in all cases.

References. H_2: Wcisło et al. (2016). CH_4: Varanasi & Chudamani (1990), Pine (1992), Fox et al. (1998), Varanasi & Tejwani (1972), Varanasi & Chudamani (1989), Grigoriev et al. (2001), Gabard et al. (2004), Manne et al. (2017), Gharib-Nezhad et al. (2019) C_2H_2, OCS, NH_3, SO_2, HF: Wilzewski et al. (2016) HCl: Wilzewski et al. (2016), Li et al. (2018) CO: Faure et al. (2013), Li et al. (2015), Mulvihill et al. (2018), Mantz et al. (2005), Predoi-Cross et al. (2016), Sinclair et al. (1998) PH_3: Kleiner et al. (2003), Levy et al. (1993), Sergent-Rozey et al. (1988), Salem et al. (2004, 2005) H_2O: Voronin et al. (2010, 2012), Barton et al. (2017b), Solodov & Starikov (2008, 2009), Petrova et al. (2013, 2012, 2016), Gamache et al. (2019) H_2CO: Nerf (1975) HCN: Mehrotra et al. (1985), Cohen & Wilson (1973), Charron et al. (1980).

Here, T_0 and P_0 are the reference temperature and pressure, respectively. γ_L^0 and n_L are the reference HWHM and temperature exponent, respectively. The latter two terms are known as pressure broadening parameters, and are dependent on the molecular species being broadened and the species causing the broadening. There is also some dependence on the rotational angular momentum quantum numbers, J, of the states involved in a particular transition.

A convolution of the two profiles given in Eqs. (1) and (3) gives a Voigt profile, which is commonly used to represent line broadening in exoplanet atmospheres:

$$f^V_{\tilde{\nu}_{fi},\alpha_D,\gamma_L}(\tilde{\nu}) = \frac{\gamma\sqrt{\ln 2}}{\pi^{\frac{3}{2}}\alpha_D}\int_{-\infty}^{\infty}\frac{e^{-y^2}\mathrm{d}y}{(\nu-y)^2+\gamma^2}, \tag{5}$$

where $\gamma = \sqrt{\ln 2}(\gamma_L/\alpha_D)$ and $\nu = \sqrt{\ln 2}(\tilde{\nu} - 2\tilde{\nu}_{fi})/\alpha_D$, with terms as defined in Eqs. (1)–(4). Technically there should be a pressure-shift of the transition wavenumber, $\tilde{\nu}_{fi}$, included in computations of line broadening. However, there are currently large experimental uncertainties associated with the relatively small number of pressure-shift values that are currently available. There is work ongoing to improve upon these parameters (e.g. Hargreaves et al. 2019; Gamache & Vispoel 2018), and we hope to include more accurate parameters such as these in future opacity calculations.

The efficient and accurate numerical computation of such a profile has been the subject of a number of publications (see, e.g. Hedges & Madhusudhan 2016; Min 2017; Schreier 2017; Grimm & Heng 2015; Yurchenko et al. 2018a; Amundsen et al. 2014). The coefficients γ_0 and n_L in Eq. (4) are dependent both on the species being broadened and on the species causing the broadening (e.g. H_2 and He are assumed to be the main broadeners in typical Hot Jupiter atmospheres (Hedges & Madhusudhan 2016)), along with the rotational angular momentum quantum numbers, J, of the states involved in a particular transition.

As mentioned in Sect. 3.1, the number of sampling points required to give well-sampled Voigt-broadened high-resolution cross sections can be estimated as a function of wavelength ν, temperature T, and pressure P, with an average number found for a given wavelength region. The Voigt width of a particular line can be approximated using the following expression (Olivero & Longbothum 1977; Rocchetto 2017):

$$\gamma_V \approx 0.5346\gamma_L + \sqrt{0.2166\gamma_L^2 + \gamma_G^2}, \tag{6}$$

where γ_L and γ_G are given by Eqs. (2) and (4), respectively. In this work, we aim for an average of four sampling points per line for the initial set of high-resolution cross sections. This is estimated using Eq. (6), as a function of pressure, temperature, and wavelength region. We use a line-wing cut-off of 500 γ_V, which is also calculated using Eq. (6) and is therefore dependent on pressure, temperature, and wavelength.

Where available, broadening parameters (γ_0 and n_L in Eq. (4)) are provided as part of the ExoMol database (see Yurchenko et al. 2017b; Barton et al. 2017a). However, in general, these broadening parameters are not well known (or given in the literature at all) for a large number of species, particularly for He and H_2 as broadeners. In this work we aim to use approximate pressure broadening parameters with He and H_2 as the broadening species (as they are thought to be the main constituents of Hot Jupiter atmospheres), at solar H_2:He ratio, based on those parameters that do exist in the literature, and using molecular properties as given in Table 2 and Tables A.1–A.11 to estimate which parameters to use for those that do not. Table 2 lists those species for which broadening parameters exist in the ExoMol database (primarily based on the work of Barton et al. 2017a). These parameters are usually given as a function of rotational angular momentum quantum number, J, for each species. Here, we have taken an average value for all values of J for a

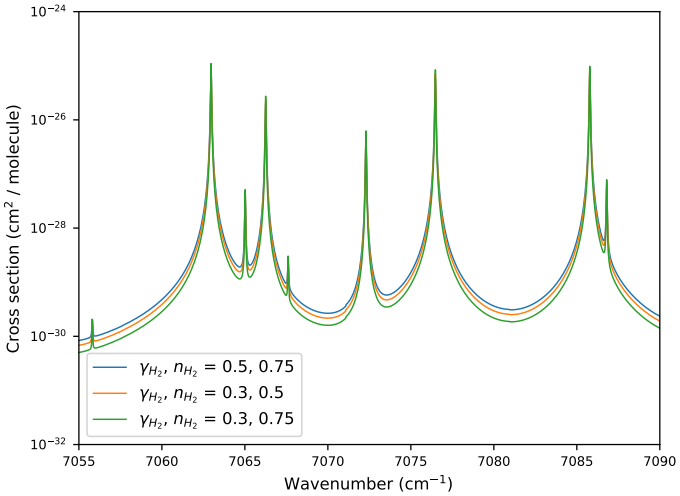

Fig. 3. HCl broadened by H_2 using different broadening parameters. The cross sections are computed at T = 1000 K and P = 0.1 bar, which are typical values for a layer of atmosphere of a Hot Jupiter exoplanet being observed in this wavelength region.

given species for broadening of both H_2 and He. When computing the cross sections, we then weight these parameters by assumed broadener abundances based on the solar H_2:He ratio. When deciding which species is most similar from a broadening point of view to those in Table 2, we consider the following factors. First, we consider the dipole moment (DM), and quadrupole moment (QM) where $DM = 0$ (Buldyreva et al. 2010a). We then also look at the general structure (e.g. linear, non-linear, diatomic), and consider molecular properties such as the centre of symmetry and interatomic distances. Of the non-polar ($DM = 0$) species in Table 2, CH_4 has $QM = 0$, H_2 has a small QM, and C_2H_2 has a relatively large QM. The other non-polar molecules are grouped accordingly, based on whether their QM is zero, low, or high. The reference for the value of the dipole moment in these tables is given where applicable. For those with no obvious value in the literature, the dipole moment was computed using MOLPRO (Werner et al. 2012), with a cc-pVTZ basis set at CASSCF level of theory (Olsen 2011). Where multiple values of dipole moment are given in the literature (depending on the level of theory used to calculate it), we used an average value. It is stressed that these values are only given as a guide towards determining which species in Table 2 is most similar to those in Tables A.1–A.11, and should not be taken as exact. For those diatomic species in Table 2 where line-by-line broadening parameters are provided (e.g. by Li et al. 2015; Wilzewski et al. 2016; Gordon et al. 2017), we use these values instead of the average parameters when computing their opacities.

Figure 3 illustrates the effect of using different broadening parameters for HCl when computing the cross sections for a pressure and temperature typical of a Hot Jupiter exoplanet being observed in the given wavelength region. The broadening is considered to be from H_2 only in this example.

Studies such as those by Hedges & Madhusudhan (2016), Rocchetto (2017), Baudino et al. (2017), Gharib-Nezhad & Line (2019), and Barstow et al. (2020) have highlighted the differences in forward models and retrievals caused by the choice of molecular broadening parameters. It is important to note that although there is a known difference between different parameters, there is still much work required in order to determine the "true" parameters, or even a good approximation, for many species. The requirement for enhanced line-broadening parameters was recently identified by Fortney et al. (2019) in their study of the need for laboratory data requirements for studies of exoplanetary atmospheres. This is the focus of various works such as Stolarczyk et al. (2020), Hartmann et al. (2018), who are improving upon the current knowledge of molecular broadening. Some detailed accounts of line-broadening theory can be found in, for example, Buldyreva et al. (2010a,b) and Wcisło et al. (2016). The latter demonstrates that H_2 has "exceptionally pronounced non-Voigt line-shape effects". We do not take these more precise effects into account in this work, but they could be considered in future work. Other intricacies have been neglected here. We note, for example, that broadening parameters are not only dependent on J, but also on the lower state symmetry (see, e.g. Gharib-Nezhad et al. 2019). However, the main focus of this work is towards useable opacities for low-resolution atmospheric retrieval studies. There are many other limiting factors when it comes to detecting molecules and making accurate determinations of their abundances. The accurate treatment of pressure effects is beyond the scope of the current work, but is planned to be significantly enhanced in future releases of the ExoMol and therefore ExoMolOP database.

3.2.1. H_2S: A broadening case study

We can compare the molecular properties of H_2S to those of the species listed in Table 2 which have some broadening parameters available in the literature. The dipole moment of H_2S is closest to HCl. However, the intermolecular distances and potential energy surface of H_2S are more similar to OCS than HCl (Johnson-III 2019), and so it is not clear which broadening parameters should be used. Here, we compute opacities using the two different sets of broadening parameters (γ_{H_2}, n_{H_2}, γ_{He}, n_{He} = 0.03, 0.75, 0.01, 0.75 and 0.05, 0.75, 0.04, 0.75, for HCl and OCS, respectively) in order to illustrate the effects of using different broadening parameters. For HCl, the average values of the broadening parameters are used from Wilzewski et al. (2016), with the exception of n_{H_2}. This latter parameter was originally sourced by Wilzewski et al. (2016) from the work of Houdeau et al. (1980), which presents negative temperature dependence exponents. As noted by Wilzewski et al. (2016), negative exponents are not impossible but they are unexpected, particularly for a simple diatomic like HCl. Negative exponents for HCl-N_2 were also previously published by Houdeau et al. (1980), which were subsequently found to be positive by Pine & Looney (1987). This gives further cause to be cautious about using the negative values. We therefore instead use the suggested default value of n_{H_2} = 0.75 for HCl. There are some values for γ_{He} (Waschull et al. 1994) and γ_{H_2} (Kissel et al. 2002; Starikov & Protasevich 2006) for the ν_2 vibrational band of H_2S. These range from 0.04–0.07 for γ_{H_2} and 0.04–0.1 for γ_{He}, which give further agreement with the values of OCS over those of HCl.

Figure 4 illustrates the difference in computed cross sections of H_2S between using the broadening parameters of Table 2 for OCS and HCl. A couple of different pressure–temperature combinations are used for comparison. It can be seen that the difference is more pronounced for lower temperatures and pressures, as was found in previous studies (Hedges & Madhusudhan 2016; Rocchetto 2017). Figure 5 illustrates forward models of a hypothetical atmosphere (computed using TauREx, Waldmann et al. 2015a,b), comparing opacities computed using these two different sets of broadening parameters. The model atmosphere is computed at 1000 K and contains H_2S only. The differences can be seen to be small, but more pronounced at higher wavelengths. For the pressures and temperatures typical of a Hot Jupiter exoplanet

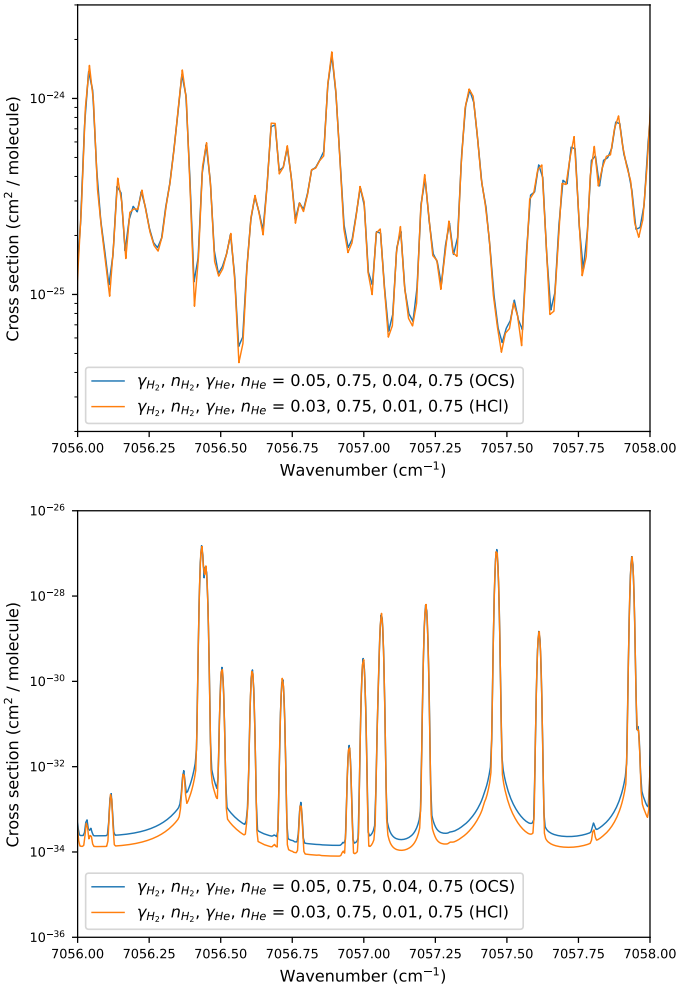

Fig. 4. H_2S broadened by H_2 and He using different broadening parameters based on values for HCl and OCS. The cross sections in the *top panel* are computed at $T = 1000$ K and ($P = 0.1$ bar), which are typical values for a layer of atmosphere of a Hot Jupiter exoplanet observed in this wavelength region. The cross sections in the *bottom panel* are computed at $T = 100$ K and $P = 1 \times 10^{-}5$ bar.

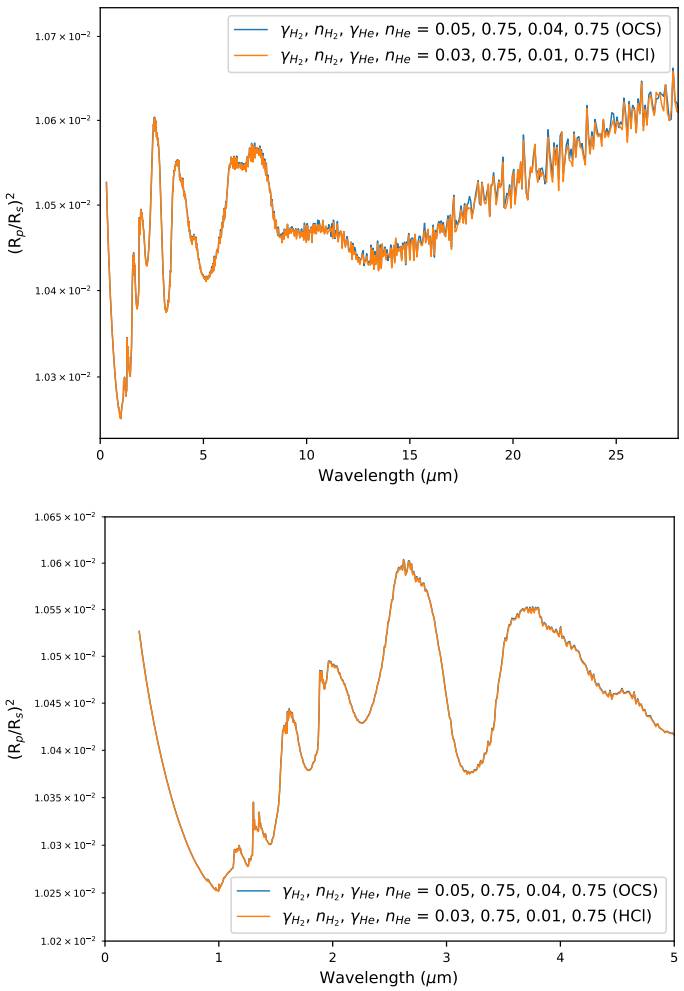

Fig. 5. Hypothetical model atmosphere of an exoplanet composed of H2S only. H_2S is broadened by H_2 and He using different broadening parameters in the two cases shown in each panel based on values for OCS and HCl. The model atmosphere is computed at $T = 1000$ K across pressures ranging from 1×10^{-5} to 1×10^{6} bar. The two panels illustrate different regions of the spectrum.

observed in the near-infrared, we do not expect the difference in broadening parameters to have a significant effect. Other uncertainties caused by for example incomplete line lists or line-wing cut-offs have been demonstrated to have a larger effect on the atmospheric spectrum by studies such as Rocchetto (2017) for example. However, the differences in opacities caused by the use of different broadening parameters should always be taken into consideration when interpreting and discussing results.

3.2.2. Comparison of broadening values used here and in other studies

Broadening parameters can be found in the literature for a small number of other species, which can then be compared to those we are using in this work. A couple of examples are given here.

The value of γ_{H_2} for C_2H_4 from Brannon & Varanasi (1992) is ~0.12 cm^{-1} atm^{-1}. We assume a value of $\gamma_{H_2} = 0.09$ cm^{-1} atm^{-1} based on the broadening parameters of C_2H_2 from Table 2.

The values of γ_{H_2} and γ_{He} for CH_3F from Lerot et al. (2006) and Grigoriev et al. (1997) are ~0.14 cm^{-1} atm^{-1} and ~0.12 cm^{-1} atm^{-1}, respectively. We assume values of $\gamma_{H_2} = 0.14$ cm^{-1} atm^{-1} and $\gamma_{He} = 0.06$ cm^{-1} atm^{-1} based on the broadening parameters of H_2CO from Table 2. Figure 6 illustrates the effects on cross sections computed using these different broadening parameters for C_2H_4 (top panel) and CH_3F (bottom panel). We note that the temperature exponents are not given in the literature for these species, and so we do not have a full set of broadening parameters to add to Table 2.

Hedges & Madhusudhan (2016) use the following metric to quantify the effect of using different broadening parameters, which we adopt here.

$$\delta = \text{median}\left(\frac{\sigma - \sigma_0}{\sigma_0}\right) \times 100, \quad (7)$$

where δ is therefore the median percent change in cross section (computed at a given pressure P and temperature T), with σ and σ_0 being the cross sections computed using two different sets of broadening parameters. Here we compute δ for cross sections of CO using the J-averaged broadening parameters of Table 2 compared to cross sections of CO using the J-dependent broadening parameters of Li et al. (2015). Here we are comparing the high-resolution cross sections before sampling to k-tables or cross sections of lower resolution. We find that δ is 0.16% for $P = 0.1$ bar and $T = 1000$ K, and that $\delta < 0.3\%$ for

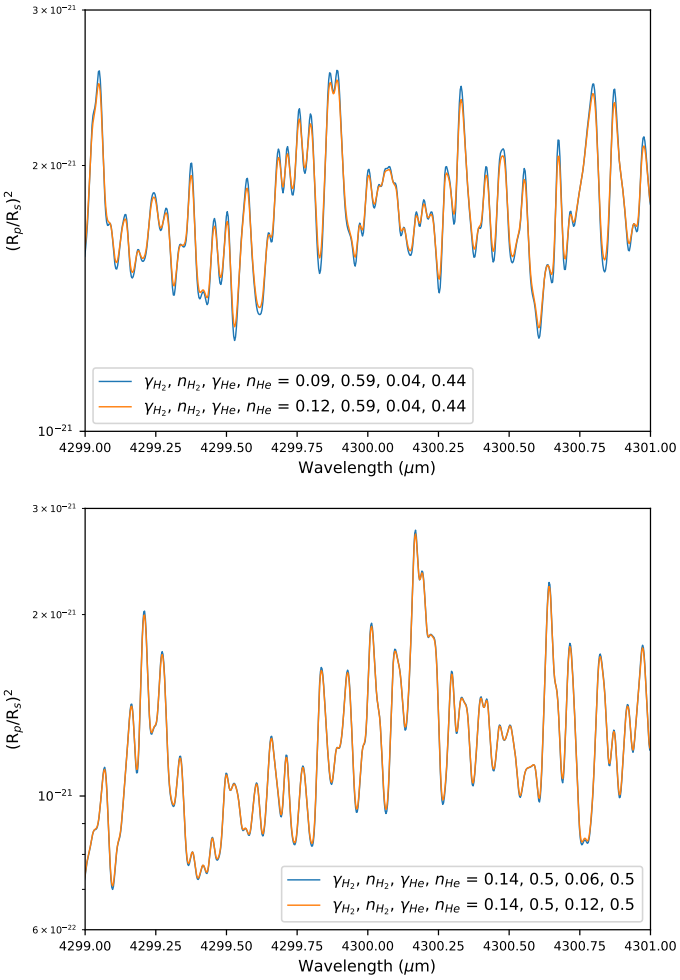

Fig. 6. C_2H_4 (*top panel*) and CH_3F (*bottom panel*) broadened by H_2 and He using different broadening parameters. The cross sections are computed at T = 1000 K and P = 0.1 bar, which are typical values for a layer of atmosphere of a Hot Jupiter exoplanet observed in this wavelength region.

all pressure–temperature combinations considered in this work. Here, δ is highest for the lowest values of pressure and temperature. Hedges & Madhusudhan (2016) find that the effect of using different broadening parameters is more pronounced at higher resolution. We therefore do not expect the approximations of broadening parameters used in this work to be a significant issue for low-resolution studies, particularly for high temperatures (>1000 K) and pressures ($>1\times10^{-3}$ bar). However, we are aware that theoretical and observational advances in the near future will mean that it will be beneficial to update ExoMolOP with more accurate parameters.

3.2.3. Atomic Na and K broadening

While the broadening parameters for molecular species are currently largely uncertain, the same is not true for the strong doublet lines in alkali metals sodium and potassium. These strong absorption features can be found in many high-temperature atmospheres; hot Jupiters (Lendl et al. 2017; Sing et al. 2014), stellar atmospheres (Takeda et al. 2012), and brown dwarfs, where they have been observed to be non-Lorentzian (Burrows et al. 2000, 2002a). Studies such as these have motivated the use of more detailed quantum chemistry calculations, which have been employed in order to accurately treat the broadening of these lines by H_2 and He for a variety of pressures and temperatures (Peach & Whittingham 2009; Allard et al. 2007, 2019; Burrows & Volobuyev 2003; Peach 2017).

In this work, the pressure- and temperature-broadened profiles for the resonance doublets of Na and K are computed using Allard et al. (2016, 2019). Future updates to these opacities intend to also consider He broadening, as outlined in Peach et al. (2020). The data for all other lines are taken from NIST Kramida et al. (2013), with Voigt broadening based on parameters inferred from Allard et al. (2007), and line-wing cut-offs computed at 4500 cm^{-1}, as recommended by Baudino et al. (2017). We do note that computing line wings out to this distance may not be wise when the profiles are not accurately known. However, preliminary tests indicate that the chosen line-wing cut-off for these non-resonance K lines makes no noticeable difference to model emission spectra of brown dwarf atmospheres (where the differences are more pronounced than in exoplanet atmospheres), as the non-resonant K lines were drowned out by other opacities. The same is assumed to be true for Na.

3.2.4. Super-lines

The super-lines method (Rey et al. 2016) is a new functionality of ExoCross (Yurchenko et al. 2018a) which allows for a huge increase in computational speed and therefore efficiency. The general principle is to compute line intensities at a given temperature T, and then to sum together the intensities of all lines within a specified spectral bin to create a so-called super line. A Voigt broadening profile is then applied to each of these super lines. As long as each of these super lines is adequately sampled then overall opacity will be conserved. We use this method when computing opacities of larger molecules, which contain many millions to billions of lines; see Tables 9 and 13. In order to ensure error transmission is kept to a minimum, we use a grid of R = 1 000 000 for the super lines (Yurchenko et al. 2017a; Tennyson et al. 2020).

3.3. K-tables

Once relatively high-resolution cross sections have been computed, it is reasonably simple to produce *k*-tables using what is known as the correlated *k*-distribution method; this method is well described in the literature (see, e.g. Lacis & Oinas 1991; Pierrehumbert 2010), and is extensively used for radiative transfer calculations in the context of planetary and substellar atmospheres (see, e.g. Irwin et al. 2008; Showman et al. 2009; Freedman et al. 2008, 2014; Lee et al. 2019; Mollière et al. 2015; Amundsen et al. 2014; Sharp & Burrows 2007; Malik et al. 2017; Drummond et al. 2016; Phillips et al. 2020). *K*-tables are generally considered faster (and more accurate for the same $R = \frac{\lambda}{\Delta\lambda}$) than cross sections, but they also come with their own assumptions and therefore limitations (see, e.g. Rocchetto 2017). However, these can be assumed to be negligible when compared to other unknowns. The general principle is to order spectral lines within a given spectral bin, producing a smooth cumulative distribution function to represent opacity, which can be more efficiently sampled. The number of points used for sampling within a given spectral bin is determined by a set of Gaussian quadrature points, which are assigned corresponding weights. These are often chosen so as to sample the extremes of the bin more finely so as not to miss the weakest and strongest lines (i.e. the distance between sampling points within a bin is not constant). One of the methods

used in this work, for example, is based on the use of Gauss Legendre polynomials (see Sect. 4 for details of the opacities produced for individual retrieval codes). *K*-tables are produced using a method of opacity sampling which enables low-resolution computations while still taking strong opacity fluctuations at high resolution into account; see, for example, Min (2017). The assumption made for the *k*-distribution method that the *k*-coefficients at each Guassian quadrature point are correlated, breaks down for inhomogeneous atmospheres (Lee et al. 2019)

4. Retrieval codes

There are several atmospheric retrieval codes in use by the exoplanetary characterisation community that are designed to solve the radiative transfer equation by looking at the propagation of radiation through a medium. We have tailored the data computed as part of this work to be directly available in the necessary format for four such retrieval codes, with no conversion necessary. These codes are ARCiS[3] (Min et al. 2020), TauREx[4] (Waldmann et al. 2015a,b; Al-Refaie et al. 2019), NEMESIS (Irwin et al. 2008), and petitRADTRANS (Mollière et al. 2019). A summary of each code is given in this section, along with the specific requirements of the data format of the input opacity files (cross sections for TauREx, and *k*-tables for the others) for each.

4.1. TauREx

TauREx is a modular Bayesian inverse retrieval suite optimised for speed (on CPU and GPU platforms) and ease of use. It was originally designed for retrievals of exoplanet transmission, emission, and phase-curve measurements (Al-Refaie et al. 2019; Changeat et al., in prep.), but has recently been extended to Solar System measurements (e.g. ExoMars Trace Gas Orbiter (TGO), Cann et al., in prep.). TauREx is publicly available[5] under a BSD license.

TauREx3 has recently been released by Al-Refaie et al. (2019) with vast speed improvements compared to previous versions of the code (Waldmann et al. 2015a,b). The currently available version of TauREx3 only has support for cross-section opacities using HDF5, pickle, and Exo-Transmit (Kempton et al. 2017) formats. The next release (version 3.1) will include *k*-table support for both petitRADTRANS and NEMESIS formats. The cross-section data can either be streamed directly or loaded into memory. The data contained in the HDF5 file are summarised in Table 3.

Table 3. Overview of the data fields contained within the HDF5 cross sections for use in the TauREx retrieval code.

Field name	Description
mol_name	Molecule name
key_iso_ll	ID for isotopologue and line list
t	List of temperatures
p	List of pressures
t.units	Units of temperature (K)
p.units	Units of pressure (bar)
bin_edges	Bin edges in wavenumbers (cm^{-1})
bin_edges.units	Units of bin edges (cm^{-1})
xsecarr	Cross-section array (*p*, *t*, *bin_centres*)
xsecarr.units	Cross-section units, cm^2/molecule
mol_mass	Molecular mass in a.m.u.
DOI	Digital Online Identifier for line list
Date_ID	ID for date of creation and version

Table 4. Overview of the data fields contained within the .fits *k*-tables for use in the ARCiS retrieval code.

Field name	Description
Tmin	Minimum temperature (K)
Tmax	Maximum temperature (K)
Pmin	Minimum pressure (bar)
Pmax	Maximum pressure (bar)
l_min	Minimum wavelength (μm)
l_max	Maximum wavelength (μm)
nT	Number of temperatures
nP	Number of pressures
nlam	Number of wavelength points
ng	Number of gauss points
kcoeff	*k*-coefficient array (*p*, *t*, *gauss*, *bin_centre*)
kcoeff_units	*k*-coefficient units (cm^2/molecule)
t	List of temperatures (K)
p	List of pressures (bar)
bin_centres	Bin centres in wavenumber (cm^{-1}) space
mol_mass	Molecular mass in a.m.u.
DOI	Digital Online Identifier for line list
mol_name	Molecule name
key_iso_ll	ID for isotopologue and line list
Date_ID	ID for date of creation and version

Notes. Here, *gauss* refers to the gauss sampling points.

4.2. ARCiS

ARCiS is an atmospheric modelling and Bayesian retrieval package (Min et al. 2020). Full details of the ARCiS code are presented in Min et al. (2020). The most important information can be found in Ormel & Min (2019). The code consists of a forward modelling part based on correlated-k molecular opacities and cloud opacities using Mie and DHS (Distribution of hollow spheres; see Min et al. 2005) computations. With ARCiS one can compute cloud formation (Ormel & Min 2019) and chemistry (Woitke et al. 2018) from physical and chemical principles. The code was benchmarked against petitCODE (Mollière et al. 2015, 2017) by Ormel & Min (2019). For the retrieval part the MULTINEST algorithm (Feroz & Hobson 2008; Feroz et al. 2009, 2013) is employed. Benchmarks for the retrieval have been performed in the framework of the ARIEL mission (Pascale et al. 2018), showing excellent agreement with multiple other retrieval codes. The Gauss sampling points used for the *k*-tables are based on Gauss Legendre polynomials. Opacities are in FITS format.

4.3. NEMESIS

NEMESIS is a planetary atmosphere radiative transfer and retrieval tool. It was originally developed for application to Solar System planets (see, e.g. Tsang et al. 2010; Fletcher et al. 2011) and has subsequently been extended and applied to exoplanets (e.g. Lee et al. 2012; Barstow et al. 2016; Krissansen-Totton et al. 2018; Irwin et al. 2020). NEMESIS can be used with either an optimal estimation (Rodgers 2000)

[3] https://www.exoclouds.com
[4] https://taurex3-public.readthedocs.io
[5] https://github.com/ucl-exoplanets/TauREx3_public

Table 5. Overview of the data fields contained within the binary *k*-tables for use in the NEMESIS retrieval code.

Field name	Description
*IREC*0	11 + 2*NG + 2 + NP + NT + NPOINT
NPOINT	Number of wavelength points
VMIN	Minimum wavelength (μm)
DELV	-1.0
FWHM	0
NP	Number of pressures
NT	Number of temperatures
NG	Number of gauss points
*IDGAS*1	NEMESIS ID for gas species
*ISOGAS*1	NEMESIS ID for gas isotopologue
G_ORDS	List of G-oordinates gauss points
G_WEIGHTS	List of weights for gauss points
Blank	Float for 0
Blank	Float for 0
p	List of pressures (bar)
t	List of temperatures (K)
bin_centres	Bin centres in wavelength (μm) space
kcoeff	*K*-coefficient array (λ, *p*, *t*, *gauss*) (10^{20} cm^2/molecule)

Table 6. Overview of the data fields contained within the HDF5 *k*-tables for use in the petitRADTRANS retrieval code.

Field name	Description
bin_centres	Bin centres in wavenumber (cm^{-1}) space
bin_edges	Bin edges in wavenumber (cm^{-1}) space
wlrange	Wavelength (μm): min, max
wnrange	Wavenumber (cm^{-1}): min, max
samples	Gauss sampling points
weights	Weights for gauss sampling points
ngauss	Number of gauss sampling points
method	Description of sampling method
kcoeff	*K*-coefficient array (*p*, *t*, *bin_centres*, *samples*)
kcoeff.units	*K*-coefficient units (cm^2 / molecule)
t	List of temperatures
p	List of pressures
t.units	Units of temperature (K)
p.units	Units of pressure (bar)
mol_mass	Molecular mass in a.m.u.
Date_ID	ID for date of creation and version
DOI	Digital Online Identifier for line list
mol_name	Molecule name
key_iso_ll	ID for isotopologue and line list

or nested sampling (PyMultiNest; Feroz & Hobson 2008; Feroz et al. 2009, 2013; Buchner et al. 2014) algorithm. It is capable of simulating a range of planetary radiative transfer scenarios, including exoplanet transit, eclipse, and phase curve spectra, and nadir and limb sounding of Solar System atmospheres; it supports the inclusion of parametrised clouds, and for some geometries multiple scattering calculations can be performed. Table 5 gives a summary of the data contained within each NEMESIS (Irwin et al. 2008) *k*-table file, which are in binary format.

4.4. petitRADTRANS

petitRADTRANS (Mollière et al. 2019) is an open-source radiative transfer code for exoplanet spectra with the Python package and implemented retrieval examples available on the code website[6]. petitRADTRANS can calculate emission and transmission spectra for cloudy and cloud-free atmospheres at high ($R = 10^6$) and low ($R = 1000$) resolution. The $R = 1000$ branch of petitRADTRANS uses opacities in the form of *k*-tables, with a wavelength grid which differs slightly from that used in the *k*-tables and cross sections produced for the other retrieval codes. The *k*-tables for petitRADTRANS are in HDF5 format, for similar reasons to those mentioned in Sect. 4.1. Table 6 gives an overview of the data fields contained within the HDF5 *k*-tables for use in the petitRADTRANS retrieval code. The code available on the website has been updated to read directly from the *k*-tables in HDF5 format that are presented in this paper. This works in a plug-and-play fashion. See the petitRADTRANS website for more information.

5. Line list sources and comments

Tables 7–14 give details for all molecular data used in this work, with tables divided into groups[7]. Included in each table is the source for the line list used for each molecule (this is what is considered to be the most complete, accurate, and up to date at the time of publication; the online ExoMol database will be updated to label the recommended line list for each molecular isotopologue if this changes); the associated minimum and maximum wavenumbers and wavelengths (E_l, E_u, λ_l, λ_u, respectively); the number of lines in the line list; the number of levels in the line list; the temperature up to which the line list is considered complete $T_{\rm max}$; and an indication for further comments, if applicable, which can be found in Sect. 5.1.2. Table 15 gives the same information for select atomic species.

5.1. Comments on tables

5.1.1. General comments

The temperature of completeness for all the MoLLIST (Bernath 2020) molecules is assumed to be 5000 K, although it is expected that most of these will not necessarily be complete, even at lower temperatures. Nevertheless, they are the best data currently available for these molecules. The opacities for these species will be updated in the future, if and when new line list data are obtained.

There are data available for some molecules not mentioned in the tables of this work, such as PF_3 (Mant et al. 2019), which is currently only computed up to a low value of the rotational angular momentum quantum number, J. It is therefore incomplete in its current state, but can be computed if requested. Readers are encouraged to contact the ExoMol team if there are particular requests for molecular data not already computed.

As previously mentioned, a small number of molecules in the HITRAN (Gordon et al. 2017) database (HF, HCl, HBr, HI, H_2) are considered applicable up to high temperatures of around 4000–5000 K (Li et al. 2013).

5.1.2. Comments on individual species

(1a) Work is underway for an updated ExoMol line list for SiO which will extend into the ultraviolet. The current line list only

[6] https://petitradtrans.readthedocs.io/en/latest/
[7] As at www.exomol.com

Table 7. Sources and properties of line list data used to compute the opacities presented in this work for metal oxides.

Species	Line list	Ref.	E_l (cm^{-1})	E_u (cm^{-1})	λ_l (μm)	λ_u (μm)	Lines	Levels	T_{max} (K)	Notes
AlO	ExoMol ATP	Patrascu et al. (2015)	100	35 000	0.29	100	4.9 million	94 000	8000	
CaO	ExoMol VBATHY	Yurchenko et al. (2016)	100	20 000	0.5	100	28.4 million	130 000	5000	
MgO	ExoMol LiTY	Li et al. (2019)	100	33 000	0.3	100	72.8 million	190 000	5000	
SiO	ExoMol EBJT	Barton et al. (2013)	100	6049	1.65	100	250 000	24 000	9000	(1a)
TiO	ExoMol TOTO	McKemmish et al. (2019)	100	30 000	0.33	100	30 million	300 000	5000	
VO	ExoMol VOMYT	McKemmish et al. (2016)	100	35 000	0.29	100	277 million	640 000	5000	

Table 8. Sources and properties of line list data used to compute the opacities presented in this work for other oxides.

Species	Line list	Ref.	E_l (cm^{-1})	E_u (cm^{-1})	λ_l (μm)	λ_u (μm)	Lines	Levels	T_{max} (K)	Notes
CO	Li 2015	Li et al. (2015)	100	23 000	0.43	100	145 000	6400	5000	
NO	HITEMP-2019	Hargreaves et al. (2019)	100	27 000	0.37	100	1.1 million	–	4000	(1b)
O_2	HITRAN	Gordon et al. (2017)	100	6997	1.43	100	290 000	–	296	
PO	ExoMol POPS	Prajapat et al. (2017)	100	12 000	0.83	100	2.1 million	43 000	5000	

Table 9. Sources and properties of line list data used to compute the opacities presented in this work for triatomics.

Species	Line list	Ref.	E_l (cm^{-1})	E_u (cm^{-1})	λ_l (μm)	λ_u (μm)	Lines	Levels	T_{max} (K)	Notes
CO_2	ExoMol UCL-4000	Yurchenko et al. (2020a)	100	20 000	0.5	100	8 billion	3.5 million	4000	(1c)
H_2O	ExoMol POKAZATEL	Polyansky et al. (2018)	100	41 200	0.24	100	6 billion	800 000	4000	(1d)
H_2S	ExoMol AYT2	Azzam et al. (2016)	100	11 000	0.91	100	115 million	220 000	2000	
HCN	ExoMol Harris	Barber et al. (2014)	100	18 000	0.56	100	34.4 million	170 000	4000	
N_2O	HITEMP-2019	Hargreaves et al. (2019)	100	12 900	0.76	100	3.6 million	–	1000	
NO_2	HITEMP-2019	Hargreaves et al. (2019)	100	4775	2.09	100	1.1 million	–	1000	
O_3	HITRAN	Gordon et al. (2017)	100	7000	1.43	100	290 000	–	296	
SiH_2	ExoMol CATS	Clark et al. (2020)	100	10 000	1.00	100	310 million	594 000	2000	
SiO_2	ExoMol OYT3	Owens et al. (2020)	100	6000	1.67	100	32.9 billion	5.7 million	3000	
SO_2	ExoMol ExoAmes	Underwood et al. (2016a)	100	8000	1.25	100	1.4 billion	3.3 million	2000	

Table 10. Sources and properties of line list data used to compute the opacities presented in this work for metal hydrides.

Species	Line list	Ref.	E_l (cm^{-1})	E_u (cm^{-1})	λ_l (μm)	λ_u (μm)	Lines	Levels	T_{max} (K)	Notes
AlH	ExoMol AlHambra	Yurchenko et al. (2018b)	100	27 000	0.37	100	36 000	1500	5000	
BeH	ExoMol Darby-Lewis	Darby-Lewis et al. (2018)	100	42 000	0.24	100	590 000	15 000	2000	
CaH	MoLLIST	Li et al. (2012)	100	22 000	0.45	100	6000	914	5000	
CrH	MoLLIST	Burrows et al. (2002b)	100	14 500	0.69	100	13,800	1600	5000	
FeH	MoLLIST	Wende et al. (2010)	100	15 000	0.67	100	93 000	3500	5000	
LiH	CLT	Coppola et al. (2011)	100	20 000	0.5	100	19 000	1100	2000	
MgH	MoLLIST	Gharib-Nezhad et al. (2013)	100	29 000	0.34	100	14 200	1300	2000	(1e)
NaH	ExoMol Rivlin	Rivlin et al. (2015)	100	37 000	0.27	100	80,000	3300	7000	
ScH	LYT	Lodi et al. (2015)	100	15 800	0.63	100	1.2 million	8500	2000	
TiH	MoLLIST	Burrows et al. (2005)	100	24 000	0.42	100	200 000	5800	5000	

considers vibration-rotation transitions and so the current maximum wavenumber was set at 6049 cm^{-1}. (1b) The HITEMP line list for NO includes data from the ExoMol NOname line list (Wong et al. 2017). (1c) The Ames line list (Huang et al. 2017) and the CDSD-4000 databank (Tashkun & Perevalov 2011) are also available for CO_2, as well as the HITEMP compilation (Rothman et al. 2010). (1d) The previous ExoMol line list for H_2O, BT2 (Barber et al. 2006), is only complete up to temperatures of 3000 K, whereas the more accurate ExoMol POKAZATEL line list Polyansky et al. (2018) is complete up

Table 11. Sources and properties of line list data used to compute the opacities presented in this work for other hydrides.

Species	Line list	Ref.	E_l (cm^{-1})	E_u (cm^{-1})	λ_l (μm)	λ_u (μm)	Lines	Levels	T_{max} (K)	Notes
CH	MoLLIST	Masseron et al. (2014)	100	39 000	0.26	100	53 000	2500	5000	
HBr	HITRAN	Li et al. (2013)	100	16 050	0.62	100	6070	–	5000	
HCl	HITRAN	Li et al. (2013)	100	20 230	0.49	100	8890	–	5000	
HF	HITRAN	Li et al. (2013)	100	32 350	0.31	100	8090	–	5000	
HI	HITRAN	Li et al. (2013)	100	14 000	0.71	100	3160	–	5000	
NH	MoLLIST	Brooke et al. (2014a, 2015) Fernando et al. (2018)	100	16 900	0.59	100	10 400	740	5000	
OH	MoLLIST	Brooke et al. (2016) Yousefi et al. (2018)	100	43 400	0.23	100	54 000	1900	5000	
PH	ExoMol LaTY	Langleben et al. (2019)	100	24 500	0.41	100	64 800	2500	4000	
SiH	ExoMol SiGHTLY	Yurchenko et al. (2018c)	100	31 000	0.32	100	1.7 million	11 800	5000	
SH	ExoMol GYT	Gorman et al. (2019)	100	39 000	0.26	100	572 145	7686	5000	

Table 12. Sources and properties of line list data used to compute the opacities presented in this work for other diatomics.

Species	Line list	Ref.	E_l (cm^{-1})	E_u (cm^{-1})	λ_l (μm)	λ_u (μm)	Lines	Levels	T_{max} (K)	Notes
AlCl	MoLLIST	Yousefi & Bernath (2018)	100	2350	4.26	100	20 200	2400	5000	
AlF	MoLLIST	Yousefi & Bernath (2018)	100	3880	2.58	100	40 500	2420	5000	
C_2	ExoMol 8states	Yurchenko et al. (2018d)	100	48 660	0.21	100	6.1 million	44 190	5000	
CaF	MoLLIST	Hou & Bernath (2018)	100	5580	1.79	100	14 800	1360	5000	
CN	MoLLIST	Brooke et al. (2014b)	100	44 200	0.23	100	195 000	7700	5000	
CP	MoLLIST	Ram et al. (2014)	100	15 000	0.67	100	28 700	2100	5000	
CS	ExoMol JnK	Paulose et al. (2015)	100	11 000	0.91	100	199 000	11 500	3000	
H_2	RACPPK	Roueff et al. (2019)	100	36 000	0.28	100	4700	300	5000	
KCl	ExoMol Barton	Barton et al. (2014)	100	2900	3.45	100	1.3 million	60 700	3000	
KF	MoLLIST	Frohman et al. (2016)	100	4000	2.49	100	10 500	1060	5000	
LiCl	MoLLIST	Bittner & Bernath (2018)	100	4840	2.07	100	26 200	2400	5000	
LiF	MoLLIST	Bittner & Bernath (2018)	100	1810	5.52	100	10 600	2400	5000	
MgF	MoLLIST	Hou & Bernath (2017)	100	5470	1.83	100	8100	900	5000	
NaCl	ExoMol Barton	Barton et al. (2014)	100	2500	4.00	100	703 000	49,000	3000	
NaF	MoLLIST	Frohman et al. (2016)	100	4990	2.01	100	7900	840	5000	
NS	ExoMol SNaSH	Yurchenko et al. (2018e)	100	38 420	0.26	100	3.2 million	31 500	5000	
PN	ExoMol YYLT	Yorke et al. (2014)	100	6500	1.54	100	140 000	14 000	5000	
PS	ExoMol POPS	Prajapat et al. (2017)	100	36 700	0.27	100	30.4 million	226 000	5000	
SiS	ExoMol UCTY	Upadhyay et al. (2018)	100	3700	2.70	100	91 600	10 000	5000	

to 4000 K. (1e) There is also a line list for MgH from ExoMol Yadin (Yadin et al. 2012). However, since it only covers the ground electronic $X^2\Sigma^+$ state, and so is less complete than the more recent MoLLIST line list of Gharib-Nezhad et al. (2013), we use the latter. (1f) Previous to the ExoMol aCeTY line list of Chubb et al. (2020b), the main sources of data for acetylene were from HITRAN (Gordon et al. 2017) and ASD-1000 (Lyulin & Perevalov 2017). The data from HITRAN are only applicable for studies performed at room temperature, and were shown in Chubb et al. (2020b) to be inadequate for high-temperature applications. ASD-1000 was a vast improvement, although there does seem to be opacity missing from some of the hot bands when compared to ExoMol aCeTY in Chubb et al. (2020b). (1g) The previous ExoMol line list for CH_4, called 10–10 (Yurchenko & Tennyson 2014), is only complete up to 1500 K. The updated 34–10 line list is therefore recommended instead. Future updates of the database will investigate using data for methane based on recent line lists from either TheoReTs (Rey et al. 2017) or HITEMP (Hargreaves et al. 2020); these are currently expected to be more accurate when considering high-resolution applications. For low-resolution applications, we expect the quality of the ExoMol line list used here to be sufficient, particularly because completeness is more important than accuracy at lower resolutions (Yurchenko et al. 2014). (1h) The energy states from Coppola et al. (2011) are used in the Amaral et al. (2019) line list for HD^+. (1i) The energy states from Engel et al. (2005) are used in the Amaral et al. (2019) line list for HeH^+. (1j) The pressure and temperature broadened profiles for the resonance doublets of Na and K are computed using Allard et al. (2016, 2019). See Sect. 3.2.3 for a discussion on the broadening profiles of these atoms.

5.2. Isotopologues

For the majority of species, we provide the opacities for the main isotopologue only, or separate opacity files for the other

Table 13. Sources and properties of line list data used to compute the opacities presented in this work for larger molecules.

Species	Line list	Ref.	E_l (cm^{-1})	E_u (cm^{-1})	λ_l (μm)	λ_u (μm)	Lines	Levels	T_{max} (K)	Notes
AsH_3	ExoMol CYT18	Coles et al. (2019a)	100	7000	1.43	100	3.6 million	4.3 million	296	
C_2H_2	ExoMol aCeTY	Chubb et al. (2020b)	100	10 000	1.00	100	4.3 billion	5.2 million	2200	(1f)
C_2H_4	ExoMol MaYTY	Mant et al. (2018)	100	7100	1.41	100	50 billion	45 million	700	
CH_3	ExoMol AYYJ	Adam et al. (2019)	100	10 000	1.00	100	2.1 billion	9.1 million	1500	
CH_3Cl	ExoMol OYT	Owens et al. (2018a)	100	6400	1.56	100	166 billion	10.2 million	1200	
CH_3F	ExoMol OYKYT	Owens et al. (2018b)	100	4700	2.13	100	1.4 billion	3.5 million	300	
CH_4	ExoMol 34to10	Yurchenko et al. (2017a)	100	18 000	0.56	100	34 billion	8.2 million	2000	(1g)
H_2O_2	ExoMol APTY	Al-Refaie et al. (2016)	100	6000	1.67	100	10 billion	7.6 million	1250	
H_2CO	ExoMol AYTY	Al-Refaie et al. (2015)	100	10 100	0.99	100	10 billion	10.3 million	1500	
HNO_3	ExoMol AIJS	Pavlyuchko et al. (2015)	100	7100	1.41	100	7 billion	17.5 million	500	
NH_3	ExoMol CoYuTe	Coles et al. (2019b)	100	20 000	0.5	100	16.9 billion	5.1 million	1500	
P_2H_2 (cis)	OY-Cis	Owens & Yurchenko (2019)	100	6000	1.67	100	5.9 billion	6 million	300	
P_2H_2 (trans)	OY-Trans	Owens & Yurchenko (2019)	100	6000	1.67	100	5.3 billion	5.9 million	300	
PH_3	ExoMol SAlTY	Sousa-Silva et al. (2015)	100	10 000	1.00	100	16.8 billion	9.8 million	1500	
SiH_4	ExoMol OY2T	Owens et al. (2017)	100	5000	2.00	100	62.7 billion	7.1 million	1200	
SO_3	ExoMol UYT2	Underwood et al. (2016b)	100	5000	2.00	100	21 billion	18.5 million	800	

Table 14. Sources and properties of line list data used to compute the opacities presented in this work for ions.

Species	Line list	Ref	E_l (cm^{-1})	E_u (cm^{-1})	λ_l (μm)	λ_u (μm)	Lines	Levels	T_{max} (K)	Notes
H_3^+	ExoMol MiZATeP	Mizus et al. (2017)	100	25 000	0.4	100	127.5 million	159 000	5000	
H_3O^+	ExoMol eXeL	Yurchenko et al. (2020b)	100	10 000	1.00	100	2.1 billion	1.2 million	1500	
HD^+	ADJSAAM	Amaral et al. (2019)	100	21 500	0.47	100	10 300	640	4000	(1h)
HeH^+	ADJSAAM	Amaral et al. (2019)	100	14 900	0.67	100	1400	180	4000	(1i)
LiH^+	CLT	Coppola et al. (2011)	100	920	10.87	100	330	75	2000	
OH^+	MoLLIST	Hodges & Bernath (2017)	100	30 300	0.33	100	12 000	820	5000	

Table 15. Sources and properties of line list data used to compute the opacities presented in this work for atoms.

Species	Line list	Ref.	E_l (cm^{-1})	E_u (cm^{-1})	λ_l (μm)	λ_u (μm)	Lines	Levels	T_{max} (K)	Notes
K	NIST	Kramida et al. (2013)	100	35 000	0.29	100	186	188	5000	(1j)
Na	NIST	Kramida et al. (2013)	100	42 000	0.24	100	523	117	5000	(1j)

isotopologues. However, for some species it is important to take natural abundances into account (see, e.g. Coursey et al. 2015). We therefore provide opacity files combined at natural abundances for the species listed in Table 16, as well as the separate isotopologue opacities.

The species included in this table may be updated if new isotopologue line lists become available (line lists can be extended to different isotopologues using the method outlined in Polyansky et al. 2017, with line positions approaching experimental accuracy for species such as H_2O). A summary of the number of isotopologues available for various line lists can be found in Tennyson & Yurchenko (2018).

6. Visible and UV

The wavelength regions covered by the data for each molecule should be carefully noted (see Tables 7–14); many of the diatomic molecules (such as PO, SiO, CrH, FeH, NH, PN, KCl, NaCl, LiCl, CS, CP, AlCl, AlF, KF, LiF, CaF, MgF) are not covered for wavelengths short of 0.67 μm, even though they are expected to have opacity in this region. Using our opacities for such species to characterise observations that span beyond this region is therefore not advised, as it could give the impression that the opacity suddenly drops off at the wavelength at which the data ends, which in practise would not be true. It is therefore desirable to have these opacities computed to higher energies (corresponding to lower wavelengths). At present, some data are available in these regions for certain molecules. The ExoMol project is planning further work on this problem which will need to consider bound-free (photodissociation) as well as bound-bound processes.

7. The ExoMolOP database

The ExoMolOP database comprises opacity data for over 80 species, details of which can be found in Tables 7–15. The data

Table 16. Species where the opacities are combined according to natural elemental abundances.

Species	Iso	NA (%)	MM (a.m.u.)
TiO	^{48}Ti^{16}O	73.7	63.94
TiO	^{46}Ti^{16}O	8.3	61.94
TiO	^{47}Ti^{16}O	7.4	62.94
TiO	^{49}Ti^{16}O	5.4	64.94
TiO	^{50}Ti^{16}O	5.2	65.94
CO	^{12}C^{16}O	98.7	27.99
CO	^{13}C^{16}O	1.1	28.99
CO	^{12}C^{18}O	2.0×10^{-3}	29.99
CO	^{12}C^{17}O	3.7×10^{-4}	28.99
CO	^{13}C^{18}O	2.2×10^{-5}	31.00
CO	^{13}C^{17}O	4.1×10^{-6}	30.00
HBr	H^{79}Br	50.7	79.93
HBr	H^{81}Br	49.3	81.92
HBr	D^{79}Br	7.9×10^{-3}	80.93
HBr	D^{81}Br	7.7×10^{-3}	82.93
HCl	H^{35}Cl	75.8	35.98
HCl	H^{37}Cl	24.2	37.97
HCl	D^{35}Cl	1.2×10^{-2}	36.98
HCl	D^{37}Cl	3.8×10^{-3}	38.98
CH_3Cl	$^{12}CH_3\,^{35}Cl$	74.9	49.99
CH_3Cl	$^{12}CH_3\,^{37}Cl$	23.9	51.99
KCl	^{39}K^{35}Cl	70.6	73.93
KCl	^{39}K^{37}Cl	22.6	75.93
KCl	^{41}K^{35}Cl	5.1	75.93
KCl	^{41}K^{37}Cl	1.6	77.92
NaCl	^{23}Na^{35}Cl	75.8	57.96
NaCl	^{23}Na^{37}Cl	24.2	59.96
LiCl	^{7}Li^{35}Cl	70.0	41.98
LiCl	^{7}Li^{37}Cl	22.4	43.98
LiCl	^{6}Li^{35}Cl	5.8	40.98
LiCl	^{6}Li^{37}Cl	1.8	42.98
AlCl	^{27}Al^{35}Cl	75.8	61.95
AlCl	^{27}Al^{37}Cl	24.2	63.95
MgO	^{24}Mg^{16}O	78.8	39.98
MgO	^{25}Mg^{16}O	9.9	40.98
MgO	^{26}Mg^{16}O	10.9	41.98
MgO	^{24}Mg^{17}O	3.0×10^{-2}	40.98
MgO	^{24}Mg^{18}O	0.2	41.98
MgH	^{24}MgH	79.0	24.99
MgH	^{25}MgH	10.0	25.99
MgH	^{26}MgH	11.0	26.99
MgF	^{24}Mg^{19}F	79.0	42.98
MgF	^{25}Mg^{19}F	10.0	43.98
MgF	^{26}Mg^{19}F	11.0	44.98

Notes. NA is the natural abundance, and MM is the molecular mass of each isotopologue.

are formatted in different ways for four different exoplanet atmosphere retrieval codes; ARCiS, TauREx, NEMESIS and petitRADTRANS (see Sect. 4), and include cross sections (at $R = \frac{\lambda}{\Delta\lambda} = 15\,000$) and k-tables (at $R = 1000$) for the 0.3–50 μm wavelength region. Voigt profiles are used to represent the broadening of molecular lines, using the broadening parameters detailed in Tables A.1–A.11, with line wings computed to 500 Voigt widths from the line centres. The pressure and temperature broadened profiles for the atomic resonance doublets of Na and K are computed using the tables of Allard et al. (2016, 2019).

7.1. Opacity data location

The opacity database is available online[8]. Opacity files can be downloaded online[9] and used directly for four retrieval codes; ARCiS, TauREx, NEMESIS and petitRADTRANS, but are intended to be sufficiently easy to manipulate for general use also.

The data will be fully integrated into ExoMol and will form part of the 2020 release which has just been completed (Tennyson et al. 2020). The opacity cross sections and k-tables will also be made available via the virtual atomic and molecular data centre (VAMDC) portal (Dubernet et al. 2010; Dubernet & Antony 2016).

7.2. Keeping opacity data up to date

The ExoMol application programming interface (API) is described in Tennyson et al. (2016), with an associated master definition file, ExoMol.all, available online[10]. The "def" files are accessed at URLs of the form `www.exomol.com/db/<molecule>/<iso-slug>/<dataset-name>/<iso-slug>__<dataset-name>.def`, with the latest dataset name for a particular molecule given in ExoMol.all. This allows for automated updates of ExoMol data to be converted to opacity (cross section and k-table) data using the HTTP WGET formalism. We use the same format as described in the ExoMol master definition files for our cross section and k-table file naming (also *key_iso_ll* within the files; see Sect. 4). Opacity files can therefore be downloaded using a URL in the following form for each of the four retrieval codes:

- `www.exomol.com/db/<molecule>/<iso-slug>/<dataset-name>/<iso-slug>__<dataset-name>.R1000_0.3-50mu.ktable.NEMESIS.kta`
- `www.exomol.com/db/<molecule>/<iso-slug>/<dataset-name>/<iso-slug>__<dataset-name>.R15000_0.3-50mu.xsec.TauREx.h5`
- `www.exomol.com/db/<molecule>/<iso-slug>/<dataset-name>/<iso-slug>__<dataset-name>.R1000_0.3-50mu.ktable.ARCiS.fits.gz`
- `www.exomol.com/db/<molecule>/<iso-slug>/<dataset-name>/<iso-slug>__<dataset-name>.R1000_0.3-50mu.ktable.petitRADTRANS.h5`

Most of the files produced have a version ID field contained within (*Date_ID*), so future updates can be tracked. For example, if the cross sections or k-tables are recomputed with improved broadening parameters, new versions will be released. It should also be noted that studies which investigate the computational feasibility versus retrieval accuracy of both k-tables and cross sections were made before some more recent computational improvements, such as more widespread use of GPUs (see, e.g. Al-Refaie et al. 2019), and similar investigations may be beneficial. Future datasets may therefore be computed at higher $R = \frac{\lambda}{\Delta\lambda}$ to reflect requirements. It should also be noted that data from high-resolution observations require line-by-line integrated opacities for analysis, as discussed below, which are

[8] www.exomol.com
[9] www.exomol.com/data/data-types/opacity/
[10] www.exomol.com/exomol.all

typically only computed in the wavelength region necessary to match observations. Such opacities are not included in the present database, but may be added in the future. For these reasons, users of the ExoMolOP database are strongly advised to reference the version of the opacities used in publications, along with the associated line list.

8. High-resolution opacity requirements

It is stressed that this database is not intended for high-resolution applications. It would be beneficial to compute a series of very high-resolution cross sections, but restricted only to wavelength regions necessary to match available observational data for cross-correlation studies; see, for example, de Kok et al. (2014), Hawker et al. (2018), Mollière & Snellen (2019), Webb et al. (2020). Currently, only a small sample of the line lists which are detailed in Tables 7–14 of Sect. 5 are suitable for use in high-resolution applications, with cross sections typically required to be sampled to a resolution of at least $R = \frac{\lambda}{\Delta\lambda} = 100\,000$. This includes those molecules which are found in the HITEMP (Rothman et al. 2010), HITRAN (Gordon et al. 2017), or MoLLIST (Bernath 2020) databases, and only those in the ExoMol (Tennyson & Yurchenko 2012; Tennyson et al. 2016) database which have been "MARVELised". MARVEL (measured active vibration-rotation energy levels) is a prodecure whereby transition wavenumbers from all available laboratory experiments are analysed together to produce a list of experimentally determined energy levels (Furtenbacher et al. 2007; Tóbiás et al. 2019). These empirical energies are then subsequently included in the MARVELised ExoMol line lists to improve their accuracy (see, e.g. Chubb et al. 2018, 2020b; McKemmish et al. 2020). As only a subsection of the energy levels, and therefore transitions, which are included in an ExoMol line list will have been MARVELised, the new ExoMol data format includes an uncertainty column in the .states file (Tennyson et al. 2020). This gives an indication of the reliability of an individual energy level, and therefore of all transitions which involve this level. A set of high-resolution cross sections for six molecular species has recently been made publicly available by Gandhi et al. (2020).

9. Conclusion

In this work we present a publicly available database of opacity cross sections and *k*-tables for molecules of astrophysical interest, ExoMolOP, which is primarily based on the latest line list data from the ExoMol (Tennyson & Yurchenko 2012; Tennyson et al. 2016), HITEMP (Rothman et al. 2010; Hargreaves et al. 2019) and MoLLIST (Bernath 2020) databases. These data are generally suitable for characterising high-temperature exoplanet or cool stellar atmospheres, and have been computed at a variety of pressures and temperatures, with a few molecules included at room temperature only from the HITRAN database. The data are formatted in different ways for four different exoplanet atmosphere retrieval codes; ARCiS (Min et al. 2020), TauREx (Waldmann et al. 2015a,b; Al-Refaie et al. 2019), NEMESIS (Irwin et al. 2008), and petitRADTRANS (Mollière et al. 2019). Opacity data for Na and K are also included using line-list data from the NIST (Kramida et al. 2013) database and the broadening scheme of Allard et al. (2016, 2019).

New opacities will be added to the ExoMolOP database as new or updated line lists become available. Updating an existing line list may include the MARVEL procedure (which can lead to noticeable differences in line positions, even at low resolution). As previously mentioned, the current ExoMolOP database is not suitable for high-resolution cross-correlation studies, but high-resolution opacities may be provided in the future alongside the current database. There are some opacities for high-resolution Doppler shift studies currently available from Gandhi et al. (2020). For the current release of the ExoMolOP database, a number of assumptions related to the broadening parameters were made, which can clearly be improved upon. The upcoming ExoMolHD project will focus on this explicitly for the next release of the database and will make use of advances in molecular broadening and line-shape theory (Stolarczyk et al. 2020; Hartmann et al. 2018). Even though the broadening parameters used in this work can clearly be improved, they are generally considered adequate for low-resolution retrieval studies. However, particular care should be taken when using these opacities in regimes where the broadening parameters may have more effect, such as for low-pressure and low-temperature environments.

Currently, only H_2 and He parameters have been used, as the primary intention is for the characterisation of Hot Jupiter exoplanets. However, future releases of the database will extend to other types of broadener, such as self-broadening, N_2, CO_2, and air, which are thought to be important in other types of planet, such as mini-Neptunes or super Earths. It is thought that, for some molecules in particular, for example H_2O, the differences between self-broadening parameters can be around seven times larger than the H_2/He parameters (Brown et al. 2005; Ptashnik et al. 2016; Gharib-Nezhad & Line 2019).

There are often different versions of computed line lists for one molecule, some with quite stark differences. Users of the ExoMolOP database are strongly urged to include citations to the line list relating to the opacities used in their publications. We include a bibtex file with the citations to all opacities included as part of the supplementary data to this work.

Acknowledgements. This project has received funding from the European Union's Horizon 2020 Research and Innovation Programme, under Grant Agreement 776403, and from the European Research Council (ERC) under the European Union's Horizon 2020 research and innovation programme under grant agreement No 758892, ExoAI. P.M. acknowledges support from the European Research Council under the European Union's Horizon 2020 research and innovation program under grant agreement No. 832428. J.T. and S.Y. thank the STFC Project No. ST/R000476/1. We gratefully acknowledge Cambridge Service for Data Driven Discovery (CSD3), part of which is operated by the University of Cambridge Research Computing on behalf of the STFC DiRAC HPC Facility (www.dirac.ac.uk). The DiRAC component of CSD3 was funded by BEIS capital funding via STFC capital grants ST/P002307/1 and ST/R002452/1 and STFC operations grant ST/R00689X/1. DiRAC is part of the National e-Infrastructure. We would like to thank Nicole Allard for providing all the data necessary to compute the broadening profiles for the Na and K resonance doublets. We thank the reviewer for their comments to improve the manuscript.

References

Adam, A. Y., Yachmenev, A., Yurchenko, S. N., & Jensen, P. 2019, J. Phys. Chem. A, 123, 4755
Allard, N. F., Kielkopf, J. F., & Allard, F. 2007, Eur. Phys. J. D, 44, 507
Allard, F., Homeier, D., & Freytag, B. 2012, Philos. Trans. R. Soc. A: Math. Phys. Eng. Sci., 370, 2765
Allard, N. F., Spiegelman, F., & Kielkopf, J. F. 2016, A&A, 589, A21
Allard, N. F., Spiegelman, F., Leininger, T., & Mollière, P. 2019, A&A, 628, A120
Al-Refaie, A. F., Yurchenko, S. N., Yachmenev, A., & Tennyson, J. 2015, MNRAS, 448, 1704
Al-Refaie, A. F., Polyansky, O. L., Ovsyannikov, R. I., Tennyson, J., & Yurchenko, S. N. 2016, MNRAS, 461, 1012
Al-Refaie, A. F., Changeat, Q., Waldmann, I. P., & Tinetti, G. 2019, ArXiv e-prints [arXiv:1912.07759]
Amaral, P. H. R., Diniz, L. G., Jones, K. A., et al. 2019, ApJ, 878, 95
Amundsen, D. S., Baraffe, I., Tremblin, P., et al. 2014, A&A, 564, A59

Azzam, A. A. A., Yurchenko, S. N., Tennyson, J., & Naumenko, O. V. 2016, MNRAS, 460, 4063
Ba, Y. A., Wenger, C., Surleau, R., et al. 2013, J. Quant. Spectr. Rad. Transf., 130, 62
Badreddine, K., El-Kork, N., & Korek, M. 2013, J. Mod. Phys., 4, 82
Barber, R. J., Tennyson, J., Harris, G. J., & Tolchenov, R. N. 2006, MNRAS, 368, 1087
Barber, R. J., Strange, J. K., Hill, C., et al. 2014, MNRAS, 437, 1828
Barstow, J. K., Aigrain, S., Irwin, P. G. J., & Sing, D. K. 2016, ApJ, 834, 50
Barstow, J. K., Changeat, Q., Garland, R., et al. 2020, MNRAS, 493, 4884
Barton, E. J., Yurchenko, S. N., & Tennyson, J. 2013, MNRAS, 434, 1469
Barton, E. J., Chiu, C., Golpayegani, S., et al. 2014, MNRAS, 442, 1821
Barton, E. J., Hill, C., Czurylo, M., et al. 2017a, J. Quant. Spectr. Rad. Transf., 203, 490
Barton, E. J., Hill, C., Yurchenko, S. N., et al. 2017b, J. Quant. Spectr. Rad. Transf., 187, 453
Baudino, J.-L., Mollière, P., Venot, O., et al. 2017, ApJ, 850, 150
Bauschlicher, C. W., Langhoff, S. R., & Komornicki, A. 1990, Theor. Chim. Acta, 77, 263
Bean, J. 2013, Follow The Water: The Ultimate WFC3 Exoplanet Atmosphere Survey, HST Proposal
Bernath, P. F. 2020, J. Quant. Spectr. Rad. Transf., 240, 106687
Bittner, D. M., & Bernath, P. F. 2018, ApJS, 235, 8
Bourgalais, J., Carrasco, N., Changeat, Q., et al. 2020, ApJ, 895, 77
Brannon, J., & Varanasi, P. 1992, J. Quant. Spectr. Rad. Transf., 47, 237
Brooke, J. S. A., Bernath, P. F., Western, C. M., van Hemert, M. C., & Groenenboom, G. C. 2014a, J. Chem. Phys., 141, 054310
Brooke, J. S. A., Ram, R. S., Western, C. M., et al. 2014b, ApJS, 210, 23
Brooke, J. S. A., Bernath, P. F., & Western, C. M. 2015, J. Chem. Phys., 143, 026101
Brooke, J. S. A., Bernath, P. F., Western, C. M., et al. 2016, J. Quant. Spectr. Rad. Transf., 138, 142
Brown, L. R., Benner, D. C., Devi, V. M., Smith, M. A. H., & Toth, R. A. 2005, J. Mol. Struct., 742, 111
Buchner, J., Georgakakis, A., Nandra, K., et al. 2014, A&A, 564, A125
Buldyreva, J., Lavrentieva, N., & Starikov, V. 2010a, Pressure Broadening and Shifting of Vibrotational Lines of Atmospheric Gases
Buldyreva, J., Lavrentieva, N., & Starikov, V. 2010b, Semi-classical Calculation of Pressure-Broadened Line Widths and Pressure-Induced Line Shifts
Bunker, P. 1974, Chem. Phys. Lett., 27, 322
Burrows, A., & Volobuyev, M. 2003, ApJ, 583, 985
Burrows, A., Marley, M. S., & Sharp, C. M. 2000, ApJ, 531, 438
Burrows, A., Burgasser, A. J., Kirkpatrick, J. D., et al. 2002a, ApJ, 573, 394
Burrows, A., Ram, R. S., Bernath, P., Sharp, C. M., & Milsom, J. A. 2002b, ApJ, 577, 986
Burrows, A., Dulick, M., Bauschlicher, C. W., et al. 2005, ApJ, 624, 988
Chan, A. C. H., & Davidson, E. R. 1968, J. Chem. Phys., 49, 727
Charron, M., Anderson, T. G., & Steinfeld, J. I. 1980, J. Chem. Phys., 73, 1494
Chen, J., Steimle, T. C., & Merer, A. J. 2007, J. Chem. Phys., 127, 204307
Chubb, K. L., Joseph, M., Franklin, J., et al. 2018, J. Quant. Spectr. Rad. Transf., 204, 42
Chubb, K. L., Min, M., Kawashima, Y., Helling, C., & Waldmann, I. 2020a, A&A, 639, A3
Chubb, K. L., Tennyson, J., & Yurchenko, S. N. 2020b, MNRAS, 493, 1531
Clark, V. H., Owens, A., Tennyson, J., & Yurchenko, S. N. 2020, J. Quant. Spectr. Rad. Transf., 246, 106929
Cohen, J. B., & Wilson, E. B. 1973, J. Chem. Phys., 58, 442
Coles, P. A., Yurchenko, S. N., Kovacich, R. P., Hobby, J., & Tennyson, J. 2019a, Phys. Chem. Chem. Phys., 21, 3264
Coles, P. A., Yurchenko, S. N., & Tennyson, J. 2019b, MNRAS, 490, 4638
Coppola, C. M., Lodi, L., & Tennyson, J. 2011, MNRAS, 415, 487
Coursey, J., Schwab, D., Tsai, J., & Dragoset, R. 2015, Atomic Weights and Isotopic Compositions (version 4.1) (Gaithersburg, MD: National Institute of Standards and Technology)
Darby-Lewis, D., Tennyson, J., Lawson, K. D., et al. 2018, J. Phys. B: At. Mol. Opt. Phys., 51, 185701
de Kok, R. J., Birkby, J., Brogi, M., et al. 2014, A&A, 561, A150
Dijkerman, H., & Ruitenberg, G. 1969, Chem. Phys. Lett., 3, 172
Drummond, B., Tremblin, P., Baraffe, I., et al. 2016, A&A, 594, A69
Dubernet, M. L., Boudon, V., Culhane, J. L., et al. 2010, J. Quant. Spectr. Rad. Transf., 111, 2151
Dubernet, M.-L., Antony, B. K., Ba1, Y. A., , et al. 2016, J. Phys. B: At. Mol. Opt. Phys., 49, 074003
Engel, E. A., Doss, N., Harris, G. J., & Tennyson, J. 2005, MNRAS, 357, 471
Falke, S., Tiemann, E., Lisdat, C., Schnatz, H., & Grosche, G. 2006, Phys. Rev. A, 74, 032503
Faure, A., Wiesenfeld, L., Tennyson, J., & Drouin, B. J. 2013, J. Quant. Spectr. Rad. Transf., 116, 79
Fernando, A. M., Bernath, P. F., Hodges, J. N., & Masseron, T. 2018, J. Quant. Spectr. Rad. Transf., 217, 29
Feroz, F., & Hobson, M. P. 2008, MNRAS, 384, 449
Feroz, F., Gair, J. R., Hobson, M. P., & Porter, E. K. 2009, CQG, 26, 215003
Feroz, F., Hobson, M. P., Cameron, E., & Pettitt, A. N. 2013, Importance Nested Sampling and the MultiNest Algorithm
Fisher, C., & Heng, K. 2018, MNRAS, 481, 4698
Fletcher, L. N., Baines, K. H., Momary, T. W., et al. 2011, Icarus, 214, 510
Fortney, J. J., Robinson, T. D., Domagal-Goldman, S., et al. 2019, Astro2020: Decadal Survey on Astronomy and Astrophysics, science white papers, 146
Fox, K., Jennings, D. E., Stern, E. A., & Hunnard, R. 1998, J. Quant. Spectr. Rad. Transf., 39, 473
Freedman, R. S., Marley, M. S., & Lodders, K. 2008, ApJS, 174, 504
Freedman, R. S., Lustig-Yaeger, J., Fortney, J. J., et al. 2014, ApJS, 214, 25
Frohman, D. J., Bernath, P. F., & Brooke, J. S. A. 2016, J. Quant. Spectr. Rad. Transf., 169, 104
Furtenbacher, T., Császár, A. G., & Tennyson, J. 2007, J. Mol. Spectrosc., 245, 115
Gabard, T., Grigoriev, I. M., Grigorovich, N. M., & Tonkov, M. V. 2004, J. Mol. Spectrosc., 225, 123
Gamache, R. R., & Vispoel, B. 2018, J. Quant. Spectr. Rad. Transf., 217, 440
Gamache, R. R., Roller, C., Lopes, E., et al. 2017, J. Quant. Spectr. Rad. Transf., 203, 70
Gamache, R. R., Vispoel, B., Renaud, C. L., Cleghorn, K., & Hartmann, L. 2019, Icarus, 326, 186
Gandhi, S., & Madhusudhan, N. 2017, MNRAS, 472, 2334
Gandhi, S., Brogi, M., Yurchenko, S. N., et al. 2020, MNRAS, 495, 224
Gharib-Nezhad, E., & Line, M. R. 2019, ApJ, 872, 27
Gharib-Nezhad, E., Shayesteh, A., & Bernath, P. F. 2013, MNRAS, 432, 2043
Gharib-Nezhad, E., Heays, A. N., Bechtel, H. A., & Lyons, J. R. 2019, J. Quant. Spectr. Rad. Transf., 239, 106649
Gordon, I. E., Rothman, L. S., Hill, C., et al. 2017, J. Quant. Spectr. Rad. Transf., 203, 3
Gorman, M., Yurchenko, S. N., & Tennyson, J. 2019, MNRAS, 490, 1652
Grigoriev, I. M., Bouanich, J. P., Blanquet, G., Walrand, J., & Lepere, M. 1997, J. Mol. Spectrosc., 186, 48
Grigoriev, I. M., Filippov, N. N., Tonkov, M. V., Gabard, T., & Doucen, R. L. 2001, J. Quant. Spectr. Rad. Transf., 69, 189
Grimm, S. L., & Heng, K. 2015, ApJ, 808, 182
Hargreaves, R. J., Gordon, I. E., Rothman, L. S., et al. 2019, J. Quant. Spectr. Rad. Transf., 232, 35
Hargreaves, R. J., Gordon, I. E., Rey, M., et al. 2020, ApJS, 247, 55
Hartmann, J.-M., Tran, H., Armante, R., et al. 2018, J. Quant. Spectr. Rad. Transf., 213, 178
Hawker, G. A., Madhusudhan, N., Cabot, S. H. C., & Gandhi, S. 2018, ApJ, 863, L11
Hedges, C., & Madhusudhan, N. 2016, MNRAS, 458, 1427
Hodges, J. N., & Bernath, P. F. 2017, ApJ, 840, 81
Holka, F., & Urban, M. 2006, Chem. Phys. Lett., 426, 252
Hou, S., & Bernath, P. F. 2017, J. Quant. Spectr. Rad. Transf., 203, 511
Hou, S., & Bernath, P. F. 2018, J. Quant. Spectr. Rad. Transf., 210, 44
Houdeau, J. P., Larvor, M., & Haeusler, C. 1980, Can. J. Phys., 58, 318
Huang, X., Schwenke, D. W., Freedman, R. S., & Lee, T. J. 2017, J. Quant. Spectr. Rad. Transf. , 203, 224
Irwin, P. G. J., Teanby, N. A., de Kok, R., et al. 2008, J. Quant. Spectr. Rad. Transf., 109, 1136
Irwin, P. G. J., Parmentier, V., Taylor, J., et al. 2020, MNRAS, 493, 106
Jacquinet-Husson, N., Armante, R., Scott, N. A., et al. 2016, J. Mol. Spectrosc., 327, 31
Johnson-III, R. D. 2019, NIST Computational Chemistry Comparison and Benchmark , https://cccbdb.nist.gov
Jørgensen, U. G. 1998, SCAN Line List Database, https://www.astro.ku.dk/~uffegj/
Juncar, P., Pinard, J., Hamon, J., & Chartier, A. 1981, Metrologia, 17, 77
Karna, S., & Grein, F. 1992, Mol. Phys., 77, 135
Kempton, E. M.-R., Lupu, R., Owusu-Asare, A., Slough, P., & Cale, B. 2017, PASP, 129, 044402
Kissel, A., Sumpf, B., Kronfeldt, H.-D., Tikhomirov, B., & Ponomarev, Y. 2002, J. Mol. Spectrosc., 216, 345
Kitzmann, D., Heng, K., Oreshenko, M., et al. 2020, ApJ, 890, 174
Kleiner, I., Tarrago, G., Cottaz, C., et al. 2003, J. Quant. Spectr. Rad. Transf., 82, 293
Kramida, A., Ralchenko, Y., & Reader, J. 2013, NIST Atomic Spectra Database - Version 5, http://www.nist.gov/pml/data/asd.cfm
Kreidberg, L., Bean, J. L., Désert, J.-M., et al. 2014, ApJ, 793, L27
Krissansen-Totton, J., Garland, R., Irwin, P., & Catling, D. C. 2018, AJ, 156, 114
Kurucz, R., & Bell, B. 1995, Kurucz Molecular Database, http://kurucz.harvard.edu/molecules.html

Lacis, A. A., & Oinas, V. 1991, J. Geophys. Res., 96, 9027
Langleben, J., Yurchenko, S. N., & Tennyson, J. 2019, MNRAS, 488, 2332
Lee, J.-M., Fletcher, L. N., & Irwin, P. G. J. 2012, MNRAS, 420, 170
Lee, G. K. H., Taylor, J., Grimm, S. L., et al. 2019, MNRAS, 487, 2082
Lee, G. K. H., Casewell, S. L., Chubb, K. L., et al. 2020, MNRAS, 496, 4674
Lendl, M., Cubillos, P. E., Hagelberg, J., et al. 2017, A&A, 606, A18
Lerot, C., Blanquet, G., Bouanich, J.-P., Walrand, J., & Lepére, M. 2006, J. Mol. Spectrosc., 238, 224
Levy, A., Lacome, N., & Tarrago, G. 1993, J. Mol. Spectrosc., 157, 172
Li, G., Harrison, J. J., Ram, R. S., Western, C. M., & Bernath, P. F. 2012, J. Quant. Spectr. Rad. Transf., 113, 67
Li, G., Gordon, I. E., Hajigeorgiou, P. G., Coxon, J. A., & Rothman, L. S. 2013, J. Quant. Spectr. Rad. Transf., 130, 284
Li, G., Gordon, I. E., Rothman, L. S., et al. 2015, ApJS, 216, 15
Li, G., Asfin, R. E., Domanskaya, A. V., & Ebert, V. 2018, Mol. Phys., 116, 3495
Li, H. Y., Tennyson, J., & Yurchenko, S. N. 2019, MNRAS, 486, 2351
Line, M. R., Wolf, A. S., Zhang, X., et al. 2013, ApJ, 775, 137
Lodi, L., Yurchenko, S. N., & Tennyson, J. 2015, Mol. Phys., 113, 1559
Lyulin, O. M., & Perevalov, V. I. 2017, J. Quant. Spectr. Rad. Transf., 201, 94
Malik, M., Grosheintz, L., Mendonça, J. M., et al. 2017, ApJ, 153, 56
Malik, M., Kitzmann, D., Mendonça, J. M., et al. 2019, AJ, 157, 170
Manne, J., Bui, T. Q., & Webster, C. R. 2017, J. Quant. Spectr. Rad. Transf., 191, 59
Mant, B. P., Yachmenev, A., Tennyson, J., & Yurchenko, S. N. 2018, MNRAS, 478, 3220
Mant, B. P., Chubb, K. L., Yachmenev, A., Tennyson, J., & Yurchenko, S. N. 2019, Mol. Phys., 1
Mantz, A., Devi, V. M., Benner, D. C., et al. 2005, J. Mol. Struct., 742, 99
Masseron, T., Plez, B., Van Eck, S., et al. 2014, A&A, 571, A47
McKemmish, L. K., Yurchenko, S. N., & Tennyson, J. 2016, MNRAS, 463, 771
McKemmish, L. K., Masseron, T., Hoeijmakers, H. J., et al. 2019, MNRAS, 488, 2836
McKemmish, L. K., Syme, A.-M., Borsovszky, J., et al. 2020, MNRAS, 497, 1081
Mehrotra, S. C., Mäder, H., Vreede, J. P. M. D., & Dijkerman, H. A. 1985, Chem. Phys., 93, 115
Mikhailenko, S. N., Babikov, Y. L., & Golovko, V. F. 2005, Atmos. Oceanic Opt., 18, 685
Min, M. 2017, A&A, 607, A9
Min, M., Hovenier, J. W., & de Koter, A. 2005, A&A, 432, 909
Min, M., Ormel, C. W., Chubb, K., Helling, C., & Kawashima, Y. 2020, A&A, 642, A28
Mizus, I. I., Alijah, A., Zobov, N. F., et al. 2017, MNRAS, 468, 1717
Mollière, P., & Snellen, I. A. G. 2019, A&A, 622, A139
Mollière, P., van Boekel, R., Dullemond, C., Henning, T., & Mordasini, C. 2015, ApJ, 813, 47
Mollière, P., van Boekel, R., Bouwman, J., et al. 2017, A&A, 600, A10
Mollière, P., Wardenier, J. P., van Boekel, R., et al. 2019, A&A, 627, A67
Mulvihill, C. R., Alturaifi, S. A., & Petersen, E. L. 2018, J. Quant. Spectr. Rad. Transf., 217, 432
Nerf, R. B. J. 1975, J. Mol. Spectrosc., 58, 451
Olivero, J. J., & Longbothum, R. L. 1977, J. Quant. Spectr. Rad. Transf., 17, 233
Olsen, J. 2011, Intern. J. Quantum Chem., 111, 3267
Ormel, C. W., & Min, M. 2019, A&A, 622, A121
Owens, A., & Yurchenko, S. N. 2019, J. Chem. Phys., 150, 194308
Owens, A., Yurchenko, S. N., Yachmenev, A., Thiel, W., & Tennyson, J. 2017, MNRAS, 471, 5025
Owens, A., Yachmenev, A., Tennyson, J., Thiel, W., & Yurchenko, S. N. 2018a, MNRAS, 479, 3002
Owens, A., Yachmenev, A., Küpper, J., Yurchenko, S. N., & Thiel, W. 2018b, Phys. Chem. Chem. Phys., 21, 3496
Owens, A., Conway, E., Tennyson, J., & Yurchenko, S. 2020, MNRAS, 495, 1927
Pascale, E., Bezawada, N., Barstow, J., et al. 2018, in Space Telescopes and Instrumentation 2018: Optical, Infrared, and Millimeter Wave, eds. M. Lystrup, H. A. MacEwen,, G. G. Fazio, et al., Int. Soc. Opt. Photonics (SPIE), 10698, 169
Patrascu, A. T., Tennyson, J., & Yurchenko, S. N. 2015, MNRAS, 449, 3613
Paulose, G., Barton, E. J., Yurchenko, S. N., & Tennyson, J. 2015, MNRAS, 454, 1931
Pavlyuchko, A. I., Yurchenko, S. N., & Tennyson, J. 2015, MNRAS, 452, 1702
Peach, G. 2017, Open Astron., 20, 516
Peach, G., & Whittingham, I. 2009, New Astron. Rev. , 53, 227 Proceedings of the VII Serbian Conference on Spectral Line Shapes (VII SCSLSA) held in Zrenjanin, Serbia June 15th-19th 2009
Peach, G., Yurchenko, S., Chubb, K., et al. 2020, Contrib. Astron. Obs. Skalnaté Pleso, 50, 193
Petrova, T. M., Solodov, A. M., Starikov, V. I., & Solodov, A. A. 2012, Mol. Phys., 110, 1493
Petrova, T. M., Solodov, A. M., Solodov, A. A., & Starikov, V. I. 2013, J. Quant. Spectr. Rad. Transf., 129, 241
Petrova, T. M., Solodov, A. M., Solodov, A. A., & Starikov, V. I. 2016, J. Mol. Spectrosc., 321, 50
Phillips, M. W., Tremblin, P., Baraffe, I., et al. 2020, A&A, 637, A38
Pierrehumbert, R. T. 2010, Radiative Transfer in Temperature-stratified Atmospheres (Cambridge University Press), 187
Pine, A. S. 1992, J. Chem. Phys., 97, 773
Pine, A., & Looney, J. 1987, J. Mol. Spectrosc., 122, 41
Polyansky, O. L., Kyuberis, A. A., Lodi, L., et al. 2017, MNRAS, 466, 1363
Polyansky, O. L., Kyuberis, A. A., Zobov, N. F., et al. 2018, MNRAS, 480, 2597
Prajapat, L., Jagoda, P., Lodi, L., et al. 2017, MNRAS, 472, 3648
Predoi-Cross, A., Esteki, K., Rozario, H., et al. 2016, J. Quant. Spectr. Rad. Transf., 184, 322
Ptashnik, I. V., McPheat, R., Polyansky, O. L., Shine, K. P., & Smith, K. M. 2016, J. Quant. Spectr. Rad. Transf., 177, 92
Ram, R. S., Brooke, J. S. A., Western, C. M., & Bernath, P. F. 2014, J. Quant. Spectr. Rad. Transf., 138, 107
Raouafi, S., Jeung, G.-H., & Jungen, C. 2001, J. Chem. Phys., 115, 7450
Rey, M., Nikitin, A. V., Babikov, Y. L., & Tyuterev, V. G. 2016, J. Mol. Spectrosc., 327, 138
Rey, M., Nikitin, A. V., & Tyuterev, V. G. 2017, ApJ, 847, 105
Rivlin, T., Lodi, L., Yurchenko, S. N., Tennyson, J., & Le Roy, R. J. 2015, MNRAS, 451, 5153
Rocchetto, M. 2017, Ph.D Thesis. University College London, London, UK
Rodgers, C. D. 2000, Inverse Methods for Atmospheric Sounding (World Scientific)
Rosmus, P., & Meyer, W. 1977, J. Chem. Phys., 66, 13
Rothman, L. S., Gordon, I. E., Barber, R. J., et al. 2010, J. Quant. Spectr. Rad. Transf., 111, 2139
Roueff, E., Abgrall, H., Czachorowski, P., et al. 2019, A&A, 630, A58
Salem, J., Bouanich, J.-P., Walrand, J., Aroui, H., & Blanquet, G. 2004, J. Mol. Spectrosc., 228, 23
Salem, J., Bouanich, J.-P., Walrand, J., Aroui, H., & Blanquet, G. 2005, J. Mol. Spectrosc., 232, 247
Schreier, F. 2017, J. Quant. Spectr. Rad. Transf., 187, 44
Sergent-Rozey, M., van Thanh, N., Rossi, I., Lacome, N., & Levy, A. 1988, J. Mol. Spectrosc., 131, 66
Sharp, C. M., & Burrows, A. 2007, ApJS, 168, 140
Showman, A. P., Fortney, J. J., Lian, Y., et al. 2009, ApJ, 699, 564
Sinclair, P., Duggan, P., Berman, R., Drummond, J. R., & May, A. 1998, J. Mol. Spectrosc., 191, 258
Sing, D. K., Wakeford, H. R., Showman, A. P., et al. 2014, MNRAS, 446, 2428
Solodov, A. M., & Starikov, V. I. 2008, Opt. Spectrosc., 105, 14
Solodov, A. M., & Starikov, V. I. 2009, Mol. Phys., 107, 43
Sousa-Silva, C., Al-Refaie, A. F., Tennyson, J., & Yurchenko, S. N. 2015, MNRAS, 446, 2337
Starikov, V. I., & Protasevich, A. E. 2006, Opt. Spectrosc., 101, 523
Stevenson, K. B., Line, M. R., Bean, J. L., et al. 2017, AJ, 153, 68
Stolarczyk, N., Thibault, F., Cybulski, H., et al. 2020, J. Quant. Spectr. Rad. Transf., 240, 106676
Suenram, R., Fraser, G., Lovas, F., & Gillies, C. 1991, J. Mol. Spectrosc., 148, 114
Takeda, Y., Kang, D.-I., Han, I., et al. 2012, PASJ, 64, 38
Tashkun, S., & Perevalov, V. 2011, J. Quant. Spectr. Rad. Transf., 112, 1403
Tennyson, J., & Yurchenko, S. N. 2012, MNRAS, 425, 21
Tennyson, J., & Yurchenko, S. N. 2018, Atoms, 6, 26
Tennyson, J., Hill, C., & Yurchenko, S. N. 2013, in 6th International Conference on Atomic and Molecular Data and their Applications ICAMDATA-2012, (New York: AIP), AIP Conf. Proc., 1545, 186
Tennyson, J., Yurchenko, S. N., Al-Refaie, A. F., et al. 2016, J. Mol. Spectrosc., 327, 73
Tennyson, J., Yurchenko, S. N., Al-Refaie, A. F., et al. 2020, J. Quant. Spectr. Rad. Transf., 255, 107228
Tóbiás, R., Furtenbacher, T., Tennyson, J., & Császár, A. G. 2019, Phys. Chem. Chem. Phys., 21, 3473
Tomasevich, G. 1970, Ph.D. Thesis, Harvard University, USA
Tsang, C. C. C., Wilson, C. F., Barstow, J. K., et al. 2010, Geophys. Lett. Res., 37
Tsiaras, A., Waldmann, I. P., Zingales, T., et al. 2018, AJ, 155, 156
Underwood, D. S., Tennyson, J., Yurchenko, S. N., et al. 2016a, MNRAS, 459, 3890
Underwood, D. S., Tennyson, J., Yurchenko, S. N., Clausen, S., & Fateev, A. 2016b, MNRAS, 462, 4300
Upadhyay, A., Conway, E. K., Tennyson, J., & Yurchenko, S. N. 2018, MNRAS, 477, 1520

Varanasi, P., & Chudamani, S. 1989, J. Quant. Spectr. Rad. Transf., 41, 335
Varanasi, P., & Chudamani, S. 1990, J. Quant. Spectr. Rad. Transf., 43, 1
Varanasi, P., & Tejwani, G. D. T. 1972, J. Quant. Spectr. Rad. Transf., 12, 849
Voronin, B. A., Mishina, T. P., Lavrentyeva, N. N., et al. 2010, J. Quant. Spectr. Rad. Transf., 111, 2308
Voronin, B. A., Lavrentieva, N. N., Lugovskoy, A. A., et al. 2012, Atmos. Oceanic Opt., 25, 27
Waldmann, I. P., Tinetti, G., Rocchetto, M., et al. 2015a, ApJ, 802, 107
Waldmann, I. P., Rocchetto, M., Tinetti, G., et al. 2015b, ApJ, 813, 13
Wang, Y., Tennyson, J., & Yurchenko, S. N. 2020, Atoms, 8, 7
Waschull, J., Kuhnemann, F., & Sumpf, B. 1994, J. Mol. Spectrosc., 165, 150
Wcisło, P., Gordon, I., Tran, H., et al. 2016, J. Quant. Spectr. Rad. Transf , 177, 75 XVIIIth Symposium on High Resolution Molecular Spectroscopy (HighRus-2015), Tomsk, Russia
Weaver, I. C., López-Morales, M., Espinoza, N., et al. 2019, ApJ, 159, 13
Webb, R. K., Brogi, M., Gandhi, S., et al. 2020, MNRAS, 494, 108
Wende, S., Reiners, A., Seifahrt, A., & Bernath, P. F. 2010, A&A, 523, A58
Werner, H.-J., Knowles, P. J., Knizia, G., Manby, F. R., & Schütz, M. 2012, WIREs Comput. Mol. Sci., 2, 242
Wilzewski, J. S., Gordon, I. E., Kochanov, R. V., Hill, C., & Rothman, L. S. 2016, J. Quant. Spectr. Rad. Transf., 168, 193
Woitke, P., Helling, C., Hunter, G. H., et al. 2018, A&A, 614, A1
Wong, A., Yurchenko, S. N., Bernath, P., et al. 2017, MNRAS, 470, 882
Yadin, B., Vaness, T., Conti, P., et al. 2012, MNRAS, 425, 34
Yorke, L., Yurchenko, S. N., Lodi, L., & Tennyson, J. 2014, MNRAS, 445, 1383
Yousefi, M., & Bernath, P. F. 2018, ApJS, 237, 8
Yousefi, M., Bernath, P. F., Hodges, J., & Masseron, T. 2018, J. Quant. Spectr. Rad. Transf., 217, 416
Yu, H., & Truhlar, D. G. 2014, J. Chem. Theory Comput., 10, 2291
Yurchenko, S. N., & Tennyson, J. 2014, MNRAS, 440, 1649
Yurchenko, S. N., Tennyson, J., Bailey, J., Hollis, M. D. J., & Tinetti, G. 2014, Proc. Nat. Acad. Sci., 111, 9379
Yurchenko, S. N., Blissett, A., Asari, U., et al. 2016, MNRAS, 456, 4524
Yurchenko, S. N., Amundsen, D. S., Tennyson, J., & Waldmann, I. P. 2017a, A&A, 605, A95
Yurchenko, S. N., Tennyson, J., & Barton, E. J. 2017b, J. Phys. Conf. Ser., 810, 012010
Yurchenko, S. N., Al-Refaie, A. F., & Tennyson, J. 2018a, A&A, 614, A131
Yurchenko, S. N., Williams, H., Leyland, P. C., Lodi, L., & Tennyson, J. 2018b, MNRAS, 479, 1401
Yurchenko, S. N., Sinden, F., Lodi, L., et al. 2018c, MNRAS, 473, 5324
Yurchenko, S. N., Szabó, I., Pyatenko, E., & Tennyson, J. 2018d, MNRAS, 480, 3397
Yurchenko, S. N., Bond, W., Gorman, M. N., et al. 2018e, MNRAS, 478, 270
Yurchenko, S. N., Mellor, T. M., Freedman, R. S., & Tennyson, J. 2020a, MNRAS, 496, 5282
Yurchenko, S. N., Tennyson, J., Miller, S., et al. 2020b, MNRAS, 497, 2340

Appendix A: Broadening tables

Table A.1. Molecular properties for the non-polar species with computed opacities presented in this work, where insufficient broadening parameters were found in the literature, and so those of CH_4 (see Table 2) were used instead.

Species	DM (d)	MM (g mol^{-1})	AN	Structure	Dipole Ref.
SiH_4	0	32.1	18	Nonpolar	

Notes. DM is the dipole moment, MM is the molar mass, and AN is the atomic number.

Table A.2. Molecular properties for the non-polar species with computed opacities presented in this work, where insufficient broadening parameters were found in the literature, and so those of H_2 (see Table 2) were used instead.

Species	DM (d)	MM (g mol^{-1})	AN	Structure	Dipole Ref.
C_2	0	12.0	12	Diatomic	Johnson-III (2019)
H_3^+	0	3.0	3	Nonpolar	Johnson-III (2019)
HD^+	0.1	3.0	2	Diatomic	Bunker (1974)

Notes. DM is the dipole moment, MM is the molar mass, and AN is the atomic number.

Table A.3. Molecular properties for the non-polar species with computed opacities presented in this work, where insufficient broadening parameters were found in the literature, and so those of C_2H_2 (see Table 2) were used instead.

Species	DM (d)	MM (g mol^{-1})	AN	Structure	Dipole Ref.
C_2H_4	0	28.0	16	Nonpolar	
CH_3	0	15.0	9	Nonpolar	Johnson-III (2019)
CO_2	0	44.0	22	Linear	
P_2H_2 (trans)	0	64.0	32	Nonpolar	
SiO_2	0	60.1	30	Linear	
SO_3	0	80.1	40	Nonpolar	

Notes. DM is the dipole moment, MM is the molar mass, and AN is the atomic number.

Table A.4. Molecular properties for the species with computed opacities presented in this work, where insufficient broadening parameters were found in the literature, and so those of CO (see Table 2) were used instead.

Species	DM (d)	MM (g mol^{-1})	AN	Structure	Dipole Ref.
AlCl	0.2	51.5	30	Diatomic	Rosmus & Meyer (1977)
AlH	0.01	28.0	14	Diatomic	
AsH_3	0.2	78.0	36	Non-linear	Johnson-III (2019)
BeH	0.2	10.0	5	Diatomic	Chan & Davidson (1968)
CH	0.4	13.0	7	Diatomic	
CN	1.5	26.0	13	Diatomic	Johnson-III (2019)
NO	0.2	30.0	15	Diatomic	Johnson-III (2019)
SiH_2	0.1	30.1	16	Non-linear	

Notes. DM is the dipole moment, MM is the molar mass, and AN is the atomic number.

Table A.5. Molecular properties for the species with computed opacities presented in this work, where insufficient broadening parameters were found in the literature, and so those of OCS (see Table 2) were used instead.

Species	DM (d)	MM (g mol^{-1})	AN	Structure	Dipole Ref.
H_2S	1	34.1	18	Polar	
N_2O	0.2	44.0	22	Linear	
NO_2	0.3	46.0	23	Non-linear	Johnson-III (2019)

Notes. DM is the dipole moment, MM is the molar mass, and AN is the atomic number.

Table A.6. Molecular properties for the species with computed opacities presented in this work, where insufficient broadening parameters were found in the literature, and so those of PH_3 (see Table 2) were used instead.

Species	DM (d)	MM (g mol^{-1})	AN	Structure	Dipole Ref.
O_3	0.5	48.0	18	Non-linear	
PH	~0.5	32.0	16	Diatomic	Johnson-III (2019)

Notes. DM is the dipole moment, MM is the molar mass, and AN is the atomic number.

Table A.7. Molecular properties for the species with computed opacities presented in this work, where insufficient broadening parameters were found in the literature, and so those of HCl (see Table 2) were used instead.

Species	DM (d)	MM (g mol^{-1})	AN	Structure	Dipole Ref.
AlF	1.5	46.0	22	Diatomic	Johnson-III (2019)
CaF	1.2	59.1	29	Diatomic	Raouafi et al. (2001)
HBr	0.8	80.9	36	Diatomic	
HeH^+	~1.3	5.0	3	Diatomic	Johnson-III (2019)
HI	0.4	127.9	54	Diatomic	
MgH	1.2	25.3	13	Diatomic	Johnson-III (2019)
O_2	0	36.0	16	Diatomic	
PS	0.6	32.0	31	Diatomic	Karna & Grein (1992)
SiH	1.2	29.1	15	Diatomic	

Notes. DM is the dipole moment, MM is the molar mass, and AN is the atomic number.

Table A.8. Molecular properties for the species with computed opacities presented in this work, where insufficient broadening parameters were found in the literature, and so those of NH_3 (see Table 2) were used instead.

Species	DM (d)	MM (g mol^{-1})	AN	Structure	Dipole Ref.
H_3O^+	~1.5	19.0	11	Non-linear	Johnson-III (2019)
P_2H_2 (cis)	1.4	64.0	32	Non-linear	

Notes. DM is the dipole moment, MM is the molar mass, and AN is the atomic number.

Table A.9. Molecular properties for the species with computed opacities presented in this work, where insufficient broadening parameters were found in the literature, and so those of HF (see Table 2) were used instead.

Species	DM (d)	MM (g mol^{-1})	AN	Structure	Dipole Ref
CP	2.1	43.0	21	Diatomic	
CS	2.0	44.1	22	Diatomic	Johnson-III (2019)
FeH	2.0	56.9	27	Diatomic	Chen et al. (2007)
LiH^+	~2	8.0	4	Diatomic	Johnson-III (2019)
MgF	1.8	43.3	21	Diatomic	
NH	0.5	15.0	8	Diatomic	Johnson-III (2019)
NS	1.8	46.1	23	Diatomic	Johnson-III (2019)
OH	1.7	17.0	9	Diatomic	Johnson-III (2019)
OH^+	~2	17.0	9	Diatomic	Johnson-III (2019)
PO	1.9	47.0	23	Diatomic	Johnson-III (2019)
ScH	1.7	46.0	22	Diatomic	Johnson-III (2019)
SiS	1.7	60.2	30	Diatomic	Johnson-III (2019)
TiH	~2	48.9	23	Diatomic	Johnson-III (2019)

Notes. DM is the dipole moment, MM is the molar mass, and AN is the atomic number.

Table A.10. Molecular properties for the species with computed opacities presented in this work, where insufficient broadening parameters were found in the literature, and so those of H_2CO (see Table 2) were used instead.

Species	DM (d)	MM (g mol^{-1})	AN	Structure	Dipole Ref.
CH_3Cl	1.9	50.5	26	Non-linear	
CH_3F	1.9	34.0	18	Non-linear	Johnson-III (2019)
H_2O_2	2.3	34.0	18	Non-linear	
HNO_3	2.2	63.0	32	Non-linear	Johnson-III (2019)

Notes. DM is the dipole moment, MM is the molar mass, and AN is the atomic number.

Table A.11. Molecular properties for the species with computed opacities presented in this work, where insufficient broadening parameters were found in the literature, and so those of HCN (see Table 2) were used instead.

Species	DM (d)	MM (g mol^{-1})	AN	Structure	Dipole Ref
AlO	4.2	43.0	21	Diatomic	Johnson-III (2019)
CaH	2.9	41.1	21	Diatomic	Holka & Urban (2006)
CaO	8.7	56.1	28	Diatomic	Yu & Truhlar (2014)
CrH	3.9	53.0	25	Diatomic	Johnson-III (2019)
KCl	10.2	74.6	36	Diatomic	Johnson-III (2019)
KF	8.6	58.1	28	Diatomic	Johnson-III (2019)
LiCl	7.1	42.4	20	Diatomic	Johnson-III (2019)
LiF	6.3	25.9	12	Diatomic	Johnson-III (2019)
LiH	5.9	8.0	4	Diatomic	Johnson-III (2019)
MgO	6.2	40.3	20	Diatomic	Johnson-III (2019)
NaCl	9.0	58.4	28	Diatomic	Johnson-III (2019)
NaF	8.1	42.0	20	Diatomic	Johnson-III (2019)
NaH	6.0	24.0	12	Diatomic	Johnson-III (2019)
PN	2.8	45.0	22	Diatomic	Johnson-III (2019)
SH	2.7	33.1	17	Diatomic	
SiO	3.1	44.1	22	Diatomic	Badreddine et al. (2013)
TiO	~3	63.9	30	Diatomic	Bauschlicher et al. (1990)
VO	3.4	66.9	31	Diatomic	Suenram et al. (1991)

Notes. DM is the dipole moment, MM is the molar mass, and AN is the atomic number.